Hematopoietic Single Cell Atlas Reveals a Diverse Repertoire of Lymphoid Cells in Larval Zebrafish

Anastasia Nizhnik[1,2], Bianca A. Ulloa[1,2], Kevyn Jackson[5], Deyou Zheng[5,6,7], Teresa V. Bowman[#1,2,3,4]

1. Albert Einstein College of Medicine, Department of Developmental and Molecular Biology Department, Bronx, NY, USA
2. Albert Einstein College of Medicine, Gottesman Institute of Stem Cell Biology and Regenerative Medicine, Bronx, NY, USA
3. Albert Einstein College of Medicine and Montefiore Medical Center, Department of Oncology, Bronx, NY, USA
4. Albert Einstein College of Medicine and Montefiore Medical Center, Department of Medicine, Bronx, NY, USA
5. Albert Einstein College of Medicine, Department of Genetics, Bronx, NY, USA
6. Albert Einstein College of Medicine and Montefiore Medical Center, The Saul R. Korey Department of Neurology, Bronx, NY, USA
7. Albert Einstein College of Medicine, Department of Neuroscience, Bronx, NY, USA

[#] To whom correspondence should be addressed.

Address: 1300 Morris Park Avenue, Bronx, NY 10461
Email: teresa.bowman@einsteinmed.edu
Phone: (718) 430-4001
Fax: (718) 430-8567

Word count: 5,997
Abstract/first paragraph word count: 149
Number of figures: 7 main, 7 supplemental figures, 6 supplemental tables
Number of references: 76

Keywords:
Hematopoietic stem cells, HSCs, HSPCs, zebrafish, differentiation, lineage tracing, single cell RNA sequencing, Innate Lymphoid Cells, ILCs, hematopoietic ontogeny

SUMMARY

During embryogenesis, hematopoietic stem cells (HSC) and HSC-independent progenitor cells form concurrently and produce overlapping and distinct immune cell types. The full repertoire of immune cells generated during development and their origin across vertebrates is incompletely elucidated. Here, we performed temporal lineage tracing of the emerging hematopoietic system during zebrafish larval development followed by single cell RNA sequencing and identified a greater diversity of lymphoid cells than previously recognized. The cells are comprised of T-lymphocytes and Innate Lymphoid-like Cells (ILCs) that are Runx1-dependent. Both T-lymphocytes and ILC-like cells depended on Il2rγ, while only T-lymphocytes depended on Rag1. The larval ILC-like cells were detected in lymphoid and mucosal organs and were responsive to viral mimicry-induced stimulation, indicating their functionality in early vertebrate life. The work provides new fundamental knowledge on the early establishment of immune hierarchies and opens the zebrafish model to broader exploration of lymphoid immunity origination and function.

INTRODUCTION

The hematopoietic system is comprised of an array of blood cells carrying out a variety of functions ranging from oxygenation to pathogen defense. Embryonic development is a critical stage for the establishment of hematopoietic and immune cell types, where multiple sequential and overlapping 'waves' of hematopoiesis produce progenitors and mature cell types[1-3]. The variety of cells generated at each wave serve a particular purpose for the proper establishment and function of lifelong hematopoietic and immune systems. Currently the field refers to two main waves of hematopoiesis: primitive and definitive[3]. The 'primitive wave' gives rise largely to macrophages and, erythrocytes[4], and neutrophils[5]. The 'definitive wave' is subdivided into an earlier pro-definitive phase and a definitive phase[6]. The pro-definitive phase progenitors generate myeloid lineage cells, megakaryocytes, NK cells[7], and B-cells. The definitive phase produces Hematopoietic Stem Cells (HSCs) that can sustain lifelong hematopoiesis.

31 During the definitive wave, hemogenic endothelial cells give rise to Hematopoietic
32 Stem and Progenitor Cells (HSPCs) which then migrate to secondary sites of
33 hematopoiesis like the fetal liver and thymus[8-10]. The emerging HSPCs are not uniform,
34 but rather heterogeneous[11-13]. Within the pool of HSPCs, there are embryonic HSC-
35 independent progenitors that emerge simultaneously with the definitive HSCs. Lineage
36 tracing studies in mice and zebrafish are establishing the connections between emerging
37 HSPCs and the mature cell types that derive from them during development[14-16].
38 However, HSCs and HSC-independent progenitors' contribution to immune and
39 hematopoietic systems remain poorly resolved due to lack of specific genetic markers.
40 The establishment and layering of the hematopoietic and immune systems during
41 development remains to be fully elucidated.
42 Embryonic HSCs and HSC-independent progenitors differentiate to produce a
43 diverse repertoire of adaptive and innate immune cells, encompassing various cells of the
44 myeloid and lymphoid lineages[2,17]. While the HSC-independent origins of tissue-resident
45 macrophages and B-1a lymphocytes are studied, origins of many other immune cell types
46 such as the Innate Lymphoid Cells (ILCs) are poorly resolved. ILCs belong to the
47 lymphoid lineage and resemble T-helper lymphocytes, however ILCs lack the adaptive
48 antigen-specific receptors characteristic of T lymphocytes[18]. ILCs are grouped into three
49 categories: ILC1, ILC2, and ILC3, paralleling the T-helper groups Th1, Th2, and Th17[19].
50 Generally, ILC1s express *Eomes* and *T-bet,* ILC2s express *Il13, Il4* and *Gata3*, while
51 ILC3s express *Il17, Il22* and *Rorc*[20]. In response to infections, ILCs can secrete cytokines
52 and recruit other immune cells[21]. The various groups of ILCs were identified in humans,
53 mice, and zebrafish models, however their embryonic origins remain unknown in
54 zebrafish and incompletely characterized in other model systems.
55 We sought to resolve the cell types generated by HSCs and HSC-independent
56 progenitors in zebrafish using a temporally inducible fluorescent reporter-based lineage
57 tracing system followed by single cell RNA sequencing (scRNA-seq). We find that
58 zebrafish HSPCs can be temporally resolved with discrete functions, whereby early
59 HSPCs produce a burst of lymphoid lineage differentiation, and late emerging HSPCs
60 generate transcriptionally different macrophages and neutrophils. Furthermore, we

uncovered that HSPCs make a diverse set of previously undescribed immune cells in zebrafish, including various groups of ILCs and several other novel immune cells. The ILC-like cells in zebrafish are present as early as 3 days-post-fertilization (dpf) and require the function of the transcription factor Runx1. Moreover, we demonstrated that viral mimicry stimulated the larval immune system with strong responses from NK/ILC1-like cells, macrophages and il2rb+T cells, which expand in numbers when treated with the TLR7/8 receptor agonist R848. To aid in future inquiries of developmental hematopoiesis and immunology, we share all scRNA-seq datasets as a resource for the research communities.

RESULTS

Lineage tracing and scRNA-seq were employed for resolving early, mid and late HSPCs in zebrafish.

During embryonic and larval development, long-lived HSCs and HSC-independent progenitors display distinct lymphoid-myeloid differentiation kinetics[14-16]. HSC-independent progenitors are the first to differentiate into mature immune cells, while HSC-derived progeny appear later[14]. While prior studies established this new paradigm, they were limited in the cell types they could examine due to technical limitations. The hematopoietic system is diverse, with numerous immune cell types that serve an array of functions and are found localized in many tissues. In a previous zebrafish lineage tracing study[14], neutrophils and thymic cells were examined, but it is unclear if the differentiation repertoire and kinetics that distinguish HSC and HSC-independent progenitors in larvae is unique to these cell types or more generalizable throughout the hematopoietic system. To address this question, we used an inducible Cre-Lox-based genetic lineage tracing approach that fluorescently labels HSPCs and their progeny, coupled with scRNA-seq to delineate the identities of labeled cells (**Figure 1A**). The Cre-Lox system is comprised of two components: *Tg(draculin:creER^{T2})*, which allows hematopoietic-selective expression of a tamoxifen-inducible Cre recombinase, and the *Tg(ubi:loxP-GFP-loxP-stop-mCherry),* which allows for ubiquitous expression of fluorescent proteins[22,23]. Upon addition of tamoxifen, Cre recombinase excises the loxP-GFP-loxP cassette, allowing for the

92 expression of mCherry. The result is permanent mCherry labeling of *draculin+* cells,
93 including HSPCs and their differentiated progeny. Previously, we determined that varying
94 the window of tamoxifen exposure during embryonic development helped to resolve
95 HSCs from the HSC-independent progenitors[14]. Here, tamoxifen-mediated Cre induction
96 of mCherry labelling is begun at either 1 dpf, 2 dpf, or 3 dpf, with hydroxytamoxifen added
97 for 20 hours (**Figure 1A**). We refer to the labeling at 1 dpf as "early-HSPCs", at 2 dpf as
98 "mid-HSPCs" and at 3 dpf as "late-HSPCs". These time points were chosen as they
99 represent early, middle, and late time points during HSPC specification and expansion
100 during zebrafish development[1]. Based on our prior study, we hypothesized that early-
101 HSPCs would be enriched for HSC-independent progenitors and mid/late-HSPCs would
102 be enriched for long-lived HSCs[14]. To identify what cells are labeled at early, mid, and
103 late induction time points, we performed scRNA-seq on mCherry-expressing cells isolated
104 from larvae 1-day-post labelling, so at 2, 3, and 4 dpf, respectively. To assess the
105 subsequent differentiated hematopoietic progeny, mCherry-expressing cells were
106 sequenced from 6 and 10 dpf larvae (**Figure 1A**). After filtering out low quality cells based
107 on standard quality control parameters in the field[24], we clustered cells in Seurat[25]. In
108 total, about 75% of mCherry-expressing cells were identified as endothelial or
109 hematopoietic, while the remaining 25% were non-hematopoietic based on top marker
110 gene expression and thus were filtered out (**Supplemental Figure 1**). As a result, 25
111 hematopoietic and immune clusters were detected across all timepoints and traces,
112 including HSCs, progenitors, and other cells of the major mature hematopoietic lineages,
113 including lymphoid, myeloid, and erythroid cells (**Figure 1B-C**, **Supplemental Figure 2,**
114 **Tables S1**). To facilitate ease of access for the community, this full dataset and all others
115 described below are available to search via a shinyapp webtool made with ShinyCell[26] at
116 https://sites.google.com/view/tvbowmanlab/developmental-hematopoiesis-atlas.
117 The HSPC clusters were identified based on the expression of *myb*, which is a
118 marker gene commonly used to assess HSPCs by *in situ* hybridization[10,27]. Expression of
119 *myb* across all time points was localized to the four stem and progenitor clusters identified
120 as Myeloid Progenitors (MyPs), Erythroid Progenitors (EryPs), Lymphoid Progenitors
121 (LyPs), and HSCs (**Figure 2A-B**). Differential expression analysis comparing HSCs to

122 EryPs, MyPs and LyPs showed distinct transcriptomes across the four clusters (**Figure**
123 **2C, Table S2**). Consistent with the lineage-enriched expression, EryPs express higher
124 levels of erythroid genes such as *klf17, alas2*, and *hemgn*, the MyP cluster express higher
125 levels of genes critical for the myeloid lineage such as *csf2rb* and *mmp9*, and the LyP
126 cluster expresses higher levels of genes associated with lymphopoiesis such as *runx3,*
127 *tcf7,* and *ccr9b* (**Table S2**). HSCs were enriched for genes encoding stem cell
128 transcription factors like *runx1*, *drl*, *tal1,* and *blf*. The abundance of each HSPC cluster
129 increased over developmental time, consistent with reported expansion of *myb*-
130 expressing HSPCs[10] (**Figure 2D**). To identify transcriptional changes occurring in HSPCs
131 as they mature during development, we did gene enrichment analysis comparing each
132 cluster over developmental time (**Figure 2E, Table S2**). We observed that the HSC
133 transcriptome was enriched for genes involved in RNA splicing and metabolism at 1-day-
134 post labeling and 10 dpf, with elevated expression of genes involved with hypoxia at 6
135 dpf. In contrast, LyPs and MyPs showed more similar changes with elevated expression
136 of genes involved with protein translation at 1-day-post labeling and protein folding at 10
137 dpf. These observations are in line with the rapid growth and protein production typically
138 associated with hematopoietic progenitors[28].
139 To visualize the early-, mid-, and late-HSPCs *in vivo*, we did confocal imaging of
140 the larval zebrafish HSPC niche termed the Caudal Hematopoietic Tissue (CHT) at 1-
141 day-post labelling (**Figure 2F**). The CHT contained the highest number of mCherry-
142 labeled cells in the early-HSPCs trace and the lowest number in the late-HSPCs trace
143 (**Figure 2F**). To identify if there were differences in the composition of HSPCs labeled by
144 each trace, we analyzed the HSPC subsets at 2, 3, and 4 dpf in the scRNA-seq dataset
145 (**Figure 2G**). Although all four populations, MyPs, LyPs, EryPs and HSCs, were detected
146 in the early-, mid-, and late-traces, the frequency of the populations was distinct. LyPs
147 were most abundant in the early-HSPC trace, HSCs were enriched in the mid-HSPC
148 trace, while EryPs were most frequent in the late-HSPC trace. These data show different
149 distributions of HSPCs across the early-, mid-, and late-HSPC pools during zebrafish
150 development.
151

152 **HSPCs differentiate into a large repertoire of immune and hematopoietic cell**
153 **types during development.**

154 By 6 and 10 dpf, HSPCs differentiate into various immune and hematopoietic
155 lineages. Consistent with our prior study[14], there is a substantial contribution of the early-
156 HSPCs to the CHT and thymus at 6 dpf, with minimal contributions from mid- and late-
157 HSPC traces, as observed by confocal imaging (**Figure 3A,A'**). The precise identity of
158 the hematopoietic cells arising in the hematopoietic tissues was unclear, so we leveraged
159 the scRNA-seq data to identify the immune cells derived from early-, mid-, and late-HSPC
160 lineage traces. Lymphoid and myeloid lineage clusters were subset and analyzed by
161 developmental timepoint (**Figure 3B**). When examined as all lymphoid clusters in
162 aggregate, a burst of differentiation from the early-HSPCs, and a concomitant decrease
163 in the proportion of LyPs, potentially due to ongoing differentiation, was observed (**Figure**
164 **3B-C**). Compared to mid- and late-HSPCs, the early-HSPCs showed a stronger
165 propensity for differentiation into lymphoid cluster 3 identified as ILC3/il2rb+Tcells. This
166 observation parallels confocal imaging, where early-HSPCs contributed significantly more
167 to the thymus than mid- or late-HSPCs (**Figure 3A**). Not all lymphoid clusters behaved
168 the same. For example, cluster 13 rag+ T cells arose at similar frequency from early- and
169 mid-HSPCs, while late-HSPCs did not generate rag+ T cells by 10 dpf (**Figure 3B-C**).

170 In contrast to the "burst" of lymphoid production, analysis of all myeloid lineage
171 clusters in aggregate showed a steady level of differentiation from all three early-, mid-,
172 and late-HSPCs traces (**Figure 3B-C'**). However, the production of myeloid lineage cells
173 by the three HSPC pools was not entirely homogenous. Late-HSPCs showed a bias
174 toward making more MyPs at 6 and 10 dpf compared to early- or mid-HSPCs, suggesting
175 that hematopoiesis maybe skewed toward myeloid lineage differentiation during later
176 larval development. Furthermore, macrophages and Antigen Presenting Cells (APCs)
177 showed different enrichments among the three traces (**Figure 3C**).

178 To determine if the immune cells derived from early-, mid- and late-HSPCs are
179 different, we did differential gene expression and functional enrichment analyses. The 10
180 dpf macrophage and neutrophil clusters were compared and showed significant
181 differences across traces (**Figure 3D,D', Table S3**). Macrophages derived from early-

182 and mid-HSPCs expressed genes involved in differentiation and NFkB-signaling, while
183 those from late-HSPCs showed an upregulation of genes in chemotaxis GO terms
184 (**Figure 3D'**). Similarly, neutrophils derived from early- and mid-HSPCs upregulated
185 oxygen transport and NFkB-signaling, while those from late-HSPCs upregulated actin
186 polymerization. To further identify genes that may be driving differentiation of
187 macrophages and neutrophils from the early-, mid- and late-HSCPs, we did pseudotime
188 analysis using psupertime, a method that takes into account the real biological timepoints
189 in pseudotime inference (**Supplemental Figure 3**)[29]. The analysis found that the cytokine
190 *il1b* appeared to be a driver of both macrophage and neutrophils differentiation from early-
191 HSPCs (**Supplemental Figure 3A,D**). The finding further indicates that macrophages
192 and neutrophils arising from early-HSPCs are different than those arising from late-
193 HSPCs.
194 In summary, our data uncovers how early-, mid- and late-HSPCs differentiate to
195 the lymphoid and myeloid lineages during larval development. These data suggest early-
196 HSPCs, which are more enriched for LyP compared to MyP, show higher propensity
197 towards the lymphoid lineage. This finding reveals layered ontogeny of lymphoid lineage
198 cells in zebrafish that is in line with other lineage tracing studies[15,16]. While all three HSPC
199 pools differentiate into macrophages and neutrophils, the gene expression analyses
200 suggest there are differences in function depending on ontogeny. The findings challenge
201 current models that infer myelopoiesis dominates earlier HSPC differentiation with
202 lymphopoietic differentiation potential arising later during developmental hematopoiesis.
203
204 **HSPCs differentiate to ILC-like and Natural Killer-like cells.**
205 In developing zebrafish, immature rag+ T-cells are the best-defined
206 lymphocytes[30,31]. However, mice and humans are known to have a larger repertoire of
207 lymphoid cells emerging during embryogenesis and fetal life. For instance, the
208 developmental formation and maturation of NK cells, ILC2s and ILC3s, as well as B1 and
209 B2 B-cell progenitors were studied in mouse models[32-34]. Non-T lymphocytes like NK cells
210 and ILCs were detected in juvenile and adult zebrafish but are not characterized in larval
211 developmental stages[24,35]. Our lineage tracing and scRNA-seq approaches allowed for a

212 more agnostic assessment of hematopoietic cells found throughout the entire larvae and
213 permitted enrichment and detection of a wider diversity of lymphoid cells than currently
214 described in larval zebrafish publications. Consistent with previous zebrafish work[31], we
215 detected rag+ T lymphocytes expressing *lck, cd4-1, cd8b, tcra,* and *tcrb* in cluster 9 of the
216 lymphoid lineage subset of cells in the scRNA-seq data (**Figure 4A-B, Table S4**). Other
217 less defined populations in larval zebrafish expressed top marker genes associated with
218 mammalian ILCs and NK cells. Cluster 0 expresses a mix of ILC3-like markers such as
219 *il7r, il23r, il17ra1a* and *tnfa*, as well as T-cell marker genes like *tcra* and *lck*. Cluster 2
220 expresses *eomesa*, *nkl.1, tbx21 (t-bet)*, and *gzm3.3* reminiscent of NK/ILC1-like cells, and
221 given the low abundance of mature markers of NK-cells like lysins and perforin, the cluster
222 may represent an immature state of NK/ILC1-like cells. Cluster 3 expresses *il13, il4,*
223 *gata3, mafa (MAF)* consistent with an ILC2-like identity. Differential expression analysis
224 between clusters 0, 2, and 3, representative of the three groups of ILCs, further highlights
225 their unique transcriptional identities (**Figure 4C, Table S4**).

226 Aside from ILC-like identity, the lymphoid subset contains a variety of T-cells,
227 progenitors, and other previously uncharacterized immune cells in larval zebrafish
228 (**Figure 4A-B**). Cluster 4 appears to be immature T cells, expressing *tcf7, mxd, cd28,* and
229 *zap70*. Cluster 8 expresses *tcrg, trdc,* indicating a possible presence of gamma-delta T-
230 cells. Cluster 7 highly expresses *gata3,* suggesting these could be ILC progenitors. The
231 putative identity of other clusters is less clear. For example, cluster 6 expresses *blnk*,
232 *ccl36.1,* and *il12rb2* possibly indicating presence of a blnk+ B-cell progenitor although
233 classic markers such as *pax5* are not detected. Cluster 5 expresses genes like *il12bb,*
234 *tox, cd59*, and *rorb*, that are expressed in many immune cell types making their identity
235 less clear thus we refer to them as cd59+ Immune Cells.

236 The various ILC types have prototypic tissue locations. For example, ILC2s can be
237 found residing in mucosal tissues like lungs and intestine and in the skin[36]. To determine
238 if larval zebrafish ILC-like cells are in tissues that align with their hypothesized identity,
239 we did whole mount *in situ* hybridization for top marker genes of ILC-like cells in 6 and 8
240 dpf larvae. We selected *eomesa* for the NK/ILC1-like cluster and *il7r* for the
241 ILC3/il2rb+Tcells. To detect ILC2-like cells, we selected the gene *si:dkey21e2.16*, which

242 is a predicted serine-type endopeptidase, and named it *swift* (**Figure 4D**). The expression
243 of *eomesa* puncta is detectable around the thymic area, consistent with thymic NK cell
244 localization[24] (**Figure 4E**). The expression of *swift* is detectable at 6 & 8 dpf along the
245 pharyngeal arches and intestines, which is consistent with mucosal localization of
246 mammalian ILC2s (**Figure 4E**). Some *swift* expressing cells were detectable in the CHT
247 (**Supplemental Figure 3G**). Lastly, *il7r* expression was localized to the thymus at 6 & 8
248 dpf, but some puncta were present outside the thymus, along the pharyngeal arches. The
249 two different locations are consistent with *il7r* marking multiple pots of cells, possibly
250 ILC3s and il2rb+Tcells. These data illustrate a previously unappreciated variety of
251 lymphoid lineage immune cells that are detectable in hematopoietic and non-
252 hematopoietic zebrafish tissues similar with their mammalian counterparts.
253
254 **Zebrafish ILC-like cells require the function of Runx1.**
255 Given the limitations of identifying novel cells by scRNA-seq alone, we functionally
256 tested if larval ILC-like cells behave consistently with their predicted identity. To determine
257 if ILC-like cells in zebrafish parallel the development of mammalian ILCs, we assessed
258 them in several mutant contexts.
259 Mammalian ILCs can emerge from 'definitive wave' embryonic progenitors that
260 pass thorough the fetal liver and genes like *Il7*, *Gata3*, *Tbx21* and *Eomes* were shown to
261 control ILC embryonic development[37]. However, it's unclear if the genetic program
262 regulating HSPC emergence is also needed for subsequent ILC development. We sought
263 to determine if Runx1 is required for ILC-like cells during embryogenesis. Runx1 is a
264 transcription factor essential for the functionality of some cells of the primitive wave and
265 for the generation of the entire definitive wave including both pro-definitive and definitive
266 phases[38-40]. Animals lacking Runx1 have a paucity of definitive HSPCs, erythrocytes,
267 macrophages, neutrophils, and T lymphocytes in both mice and zebrafish[41-43]. To
268 determine if ILC-like cells require the function of Runx1, we performed hematopoietic
269 lineage tracing in the *runx1*^{W84X} zebrafish mutants[41]. Heterozygous *runx1*^{W84X} fish
270 containing either *Tg(drl:creER*^{T2}*)* or *Tg(ubi:loxP-GFP-loxP-stop-mCherry)* were crossed
271 to obtain *runx1* wild-type, heterozygous, and homozygous mutant embryos containing

272 both the tamoxifen-inducible Cre enzyme and the switch cassette
273 *Tg(drl:creER^{T2},ubi:Switch)* (**Figure 5A**). Given that the largest proportion of lymphoid
274 lineage cells were detected in the early-HSPC cohort, we did confocal imaging and
275 scRNA-seq using the early-HSPCs labeling time point with final analysis at 6 dpf.
276 By confocal imaging, early-HSPC-derived mCherry-expressing cells were
277 significantly reduced in hematopoietic sites like the thymus and caudal hematopoietic
278 tissue, as well as along the intestine in the *runx1^{W84X}* homozygous mutants (**Figure 5B**).
279 Loss of thymic signal suggested that lymphoid lineage cells were depleted in mutants,
280 and loss of signal in the caudal hematopoietic tissue suggested a depletion of other
281 lineages like erythroid, myeloid, and HSPCs.
282 To determine which specific hematopoietic and immune cells are dependent on
283 Runx1, we performed scRNA-seq on mCherry+ cells isolated from *runx1^{W84X}*
284 homozygous mutants and their siblings at 6 dpf (**Figure 5C, Supplemental Figure 4A-**
285 **E, Table S5**). To identify the homozygous mutants for sequencing, larvae were scored
286 for a loss of thymic mCherry signal at 6 dpf by imaging. We selected *runx1^{W84X}*
287 homozygous mutants and unaffected siblings [mix of wildtype (+/+) and heterozygous (+/-
288)] based on this metric and confirmed the genotype of single cell suspensions using a
289 SNP-based genotyping strategy. The scRNA-seq data revealed that *runx1^{W84X}*
290 homozygous mutants lack the following lineages: HSPCs, neutrophils and macrophages,
291 and all the lymphoid lineage cells including rag+ T cells, and ILC-like clusters (**Figure 5C-**
292 **D, Supplemental Figure 4E**). As anticipated, the clusters identified in a wild-type control
293 dataset from prior experiment were present in the sibling controls (**Figure 5C**). Despite
294 the depletion of most hematopoietic cells in *runx1* homozygous mutants, some
295 erythrocytes and thrombocytes were still detectable in 6 dpf mutants. Erythrocytes are
296 longer lived cells that can arise from both primitive and definitive hematopoietic waves,
297 and prior work in murine models also suggest that megakaryopoiesis can occur from
298 primitive wave hematopoietic progenitors[44,45]. It is likely that the primitive erythrocytes and
299 thrombocytes are directly labeled in the early-HSPC trace due to the expression of
300 *Tg(drl:creER^{T2})*, and appear Runx1-independent[14]. Whole mount *in situ* RNA
301 hybridization for *eomesa, swift,* and *il7r* in *runx1^{W84X}* mutants corroborated the significant

302 reduction of NK/ILC1-like, ILC2-like, and ILC3/il2rb+Tcells in the homozygous *runx1*^{W84X}
303 mutants at 6 dpf (**Figure 5E, Supplemental Figure 4F**). These findings show the Runx1
304 dependency of the newly identified lymphocytes including ILC-like cells.
305
306 **Zebrafish ILC-like cells show similar dependencies on Il2rγ and Rag1 as**
307 **mammalian ILCs.**
308 ILCs and adaptive T-lymphocytes, specifically *cd4+* T-helper cells, express similar
309 genes[18]. Therefore, identification of ILCs solely based on gene expression is inadequate
310 to distinguish ILCs from T-helper cells. ILCs and T-lymphocytes show some common and
311 unique genetic dependencies. In humans and in mice, both ILCs and T-lymphocytes
312 depend on the function of interleukin 2 common gamma chain (IL2Rγ) because the
313 immune cells express various interleukins that require IL2RG as a co-receptor[46]. Unlike
314 T-lymphocytes, ILCs lack antigen-specific receptors, and therefore do not require the
315 function of Rag1 and Rag2 recombinase enzymes for their development[19]. To better
316 parse out ILCs from T-cells in larval zebrafish, we assessed the cells in *il2rga*^{Y91fs}
317 homozygous mutants[47] and *rag1* mutagenized zebrafish. We anticipated that zebrafish
318 ILC-like cells would be diminished in an *il2rga* mutant and unaffected by mutagenesis of
319 *rag1*.
320 In zebrafish, Il2rγ is encoded by the duplicated genes *il2rga* and *il2rgb*, however
321 only *il2rga* functions during developmental lymphopoiesis[48]. We used the *il2rga*^{Y91fs}
322 zebrafish mutants to determine if larval ILCs require the function of Il2rγ. Heterozygous
323 *il2rga*^{Y91fs} fish containing either *Tg(drl:creER*^{T2}*)* or *Tg(ubi:loxP-GFP-loxP-stop-mCherry)*
324 were crossed to obtain *il2rga* wild-type, heterozygous, and homozygous embryos with
325 both the tamoxifen-inducible Cre enzyme and the switch cassette (**Figure 6A**). Early-
326 HSPCs were labeled at 1 dpf and the mCherry expressing progeny were analyzed at 8
327 dpf using confocal imaging. In homozygous *il2rga*^{Y91fs} mutants, mCherry-expressing cells
328 were significantly reduced in the thymus and intestine compared with the wild-type and
329 heterozygous siblings (**Figure 6B**). However, mCherry-expressing cells in the CHT were
330 unaffected by the loss of *il2rga* consistent with undetectable expression of ILC1 and ILC3
331 markers (data not shown) and minimal ILC2 marker expression in this hematopoietic

332 tissue (**Supplemental Figure 4F**). To further parse out if ILC-like cells are dependent on
333 *il2rga*, we did *in situ* hybridization for *eomesa, swift,* and *il7r* at 6 dpf and showed reduced
334 expression of all three markers in *il2rga*^{Y91fs} homozygous mutants compared to wild-type
335 and heterozygous siblings (**Figure 6C, Supplemental Figure 5A**).
336 To distinguish ILCs from T-lymphocytes, we mutagenized the *rag1* locus using
337 CRISPR/Cas9 in *Tg(drl:creER*^{T2}*,ubi:Switch)* zebrafish larvae and then assessed T-
338 lymphocytes and ILCs **(Supplemental Figure 5B-D)**. To control for off-target effects from
339 mutagenesis, we compared *rag1* crispants to larvae mutagenized at the *slc24a5 golden*
340 locus, a non-essential gene which is required for melanin pigmentation in zebrafish[49]. In
341 *rag1* crispants, T-cells were decreased when assessed by imaging of the T-cell
342 fluorescent reporter *Tg(rag2:mCherry)* and by *in situ* hybridization for *rag1* and *tcra*,
343 functionally confirming robust *rag1* mutagenesis (**Supplemental Figure 5C-D**).
344 To assess all lymphopoiesis in *rag1* and control *slc24a5* crispants, we performed
345 scRNA-seq on the early-HSPC trace-derived mCherry-expressing cells isolated from 8
346 dpf larvae (**Figure 6A**). We hypothesized that Rag1-independent cells would show no
347 change in abundance in the *rag1* crispants, while Rag1-dependent cells like T-
348 lymphocytes would be diminished. As anticipated, cluster 8 identified as *rag*-expressing
349 T-lymphocytes were diminished in *rag1* crispants (**Figure 6D,E, Table S6**). The T-cell
350 identity of the newly discovered il2rb+ T cells was confirmed by their decreased
351 abundance in *rag1* crispants. Based on gene expression, clusters 1 and 7 appear to be
352 the ILC3s and T-cells observed as cluster 0 in the original HSPC trace dataset (**Figure
353 4A**), but possibly due to the *rag1* genetic perturbation, the two cell types separated in this
354 dataset (**Figure 6D**). Clusters 2, 6, 7, 9, and 11 were identified as ILC-like based on top
355 marker gene expression, and were still present in high abundance in *rag1* crispants in
356 accordance with ILCs not requiring Rag enzymes for their development (**Figure 6D,E,
357 Supplemental Figure 5E,F**). ILC2-like cells are represented by two clusters in this
358 dataset, clusters 6 and 9. Concordant with a recent mammalian study[50], we noted an
359 increase in Cluster 9, which has more *il13*-expressing ILC2s than in the control. Clusters
360 3 and 4 identified as cd59+ and blnk+ immune cells, respectively, are also Rag1-
361 independent, indicating that they are likely not T-lymphocytes but rather another type of

specialized immune cells. *In situ* hybridization for markers of ILC1/NK-like and ILC2-like cells, *eomesa*, and *swift* respectively, confirmed Rag1 independence (**Figure 6F, Supplemental Figure 5G**). However, expression of *il7r* by *in situ* decreased in *rag1* crispants, indicating that the cells marked by *il7r* include T-lymphocytes consistent with the expression of *il7r* in both il2rb+ Tcell cluster 1 and ILC3-like cluster 7 (**Table S6**). In summary, transcriptionally detected ILC-like cells in zebrafish show genetic dependencies consistent with their proposed identity, and in agreement with mammalian ILCs.

Viral mimicry stimulates ILC-like expansion in zebrafish larvae.

Innate lymphocytes participate in the immune system response to pathogenic insults by viruses, bacteria, and helminths[21]. We sought to test the functionality of larval ILC-like cells as well as other immune cells by simulating a viral infection in zebrafish larvae. In the scRNA-seq datasets, the ILC1/NK-like cluster expresses TLR receptor 8 (*tlr8b*) which is a receptor known to selectively sense single-stranded RNA (ssRNA) viruses like SARS-CoV2 and influenza[51] (**Supplemental Figure 6E**). To mimic a ssRNA viral infection, we chose the TLR7/8 agonist R848 (Resiquimod) because studies showed adult mammalian NK-cells respond to this stimulant[52]. Furthermore, R848 can induce a strong immune response by prompting activation of macrophages[53,54], however the effect of R848 agonist on the larval lymphoid lineage in zebrafish is unknown.

First, we sought to test the effect of R848 on larval immune cells broadly using imaging. Early-HSPCs were labeled with mCherry and then larvae were treated with 28.5 μM R848 at 6 dpf and subjected to confocal imaging at 8 dpf. (**Figure 7A**). The treatment window of 6 – 8 dpf was selected to capture the potentially more mature ILCs as they had higher abundance in the scRNA-seq at the older timepoints. At 8 dpf, the R848-treated larvae had a significant increase in mCherry signal in the thymus and CHT as well as an increased number of puncta in the intestine as compared to untreated controls (**Figure 7B**).

Next, to determine which immune cells and ILC types respond to the viral mimic, we did scRNA-seq on early-HSPC-derived mCherry-expressing cells from 8 dpf *slc24a5*

392 crispant controls and *rag1* crispants treated with R848 (**Supplemental Figure 6A-D**). As
393 anticipated, there is a significant expansion of macrophage clusters 5, 9, and 18 in R848-
394 treated larvae at 8 dpf (**Figure 7C-D, Supplemental Figure 7B**). Gene enrichment
395 analysis revealed R848 induced transcriptional changes in these clusters that are
396 concordant with metabolic changes and defense response activation (**Supplemental**
397 **Figure 7A, Table S6**). Based on expression of *tlr8b*, we expected that R848 would elicit
398 a response from the ILC1/NK-like cluster (**Supplemental Figure 6E,F**). Indeed, there is
399 an expansion of cluster 12 identified as ILC1/NK-like (**Figure 7C-D, Supplemental**
400 **Figure 7B**) in both *slc24a5* controls and in *rag1* crispants treated with R848. Gene
401 enrichment analysis of differentially expressed genes in ILC1/NK-like cells between
402 control and R848 treated larvae showed an upregulation of actin polymerization and
403 motility GO terms, consistent with a study showing increased migration of NK cells in
404 responses to R848[55](**Figure 7E, Table S6**). We also observed an expansion of cluster 6
405 il2rb+ T cells, in all R848-treated samples. Lastly, cluster 21 identified as ILC2-like was
406 diminished in R848-treated larvae, with about a 3-fold decrease in the number of cells
407 between controls (153 cells) and R848 treated (45 cells). Our observation is in agreement
408 with a study showing suppression of ILC2s in response to R848[56](**Figure 7C,D**).
409 To confirm the cellular effects of R848 as observed by scRNA-seq, we did *in situ*
410 hybridization in whole larvae at 8 dpf for ILC-like marker genes, *eomesa*, *swift*, and *il7r*.
411 (**Figure 7F**). Expression of *eomesa* was significantly increased by R848 treatment,
412 including along the pharyngeal arches, suggesting that ILC1/NK-like cells are responsive
413 during larval development. The expression of ILC2 marker gene *swift* was unchanged
414 between controls and R848 treated, counter to what was observed in scRNA-seq (**Figure**
415 **7F, Supplemental Figure 7C**). Lastly, the expression of *il7r* in the thymus was
416 significantly increased in response to R848 agonist (**Figure 7F**). The *in situ* hybridization
417 result supports the observed expansion of cluster 6 il2rb+Tcells in the sequencing data.
418 Together, our findings indicate that larval ILC-like cells in zebrafish have the same
419 dependencies as established in murine and human studies. Larval zebrafish ILCs require
420 Il2rγ but not Rag1 and are responsive to a viral-like immune challenge. Identification of
421 the various immune system populations equivalent to mammalian systems shows that

422 larval zebrafish represent a valid and tractable model for addressing broader questions
423 about immunity and disease.
424
425 **DISCUSSION**
426
427 In this paper, we show that HSPCs arising at different developmental windows
428 have distinctive kinetics of differentiation to the lymphoid and myeloid lineages. Using
429 scRNA-seq, we uncovered embryonic progenitors that have myeloid, lymphoid, or
430 erythroid biases. The broad characterization of cells made by HSPCs during development
431 revealed the existence of a wider variety of immune cells in larvae. We also observed
432 numerous previously unknown lymphoid populations including ILCs. Zebrafish ILCs have
433 similar genetic dependencies as mammalian counterparts, and larval ILCs can respond
434 to a viral mimic by at least 6 dpf. The scRNA-seq datasets are available via an online
435 search tool for the zebrafish, hematology, and immunology communities to facilitate
436 further study of the various immune cells identified.
437 The layered nature of developmental hematopoiesis makes it challenging to
438 examine the distinct qualities of each wave of stem and progenitor cells as well as their
439 progeny. The early, mid and late HSPC lineage tracing results help illuminate these
440 features and uncovered distinct differentiation dynamics. Early HSPCs showed a more
441 rapid differentiation into lymphoid cells, especially il2rb+ T cells and ILC3s. Meanwhile
442 late-HSPCs differentiate at a slower pace and with a more limited collection of lymphoid
443 cells compared to early and mid HSPCs. Murine studies are in line with our finding, where
444 an early wave of ILC3s arising from the hemogenic endothelium and seed the nascent
445 thymus during embryogenesis[57,58]. From the myelopoietic perspective, all three HSPC
446 traces appeared to produce myeloid cells at a similar steady rate. It could be interpreted
447 that the early and late wave myeloid cells are derived from primitive and definitive waves,
448 respectively. However, early HSPC-derived myeloid cells were depleted in *runx1*^{W84X}
449 homozygous mutants, which do not display decreases in primitive myeloid cells[41]. This
450 finding indicates the myeloid cells detected in the early HSPC trace are likely of definitive
451 origin implying the difference between early and late HSPC derived cells is something
452 new. The increase in MyPs in the late-HSPCs trace suggests distinctive definitive myeloid

453 differentiation across zebrafish larval development. Further supporting this model is the
454 observation that the myeloid cells derived from early *versus* late HSPCs have distinct
455 gene expression profiles. The late-HSPC-derived macrophages and neutrophils showed
456 different gene enrichment from those derived from early and mid HSPCs in concordance
457 with other work in the field indicating origin informs functional properties[59]. Future
458 assessments of early, mid, and late HSPC-derived myeloid progeny across diverse
459 hematopoietic and immune organs in adulthood could help elucidate how different
460 embryonic waves shape the adult immune and hematopoietic systems.

461 Prior to this study, the array of cells routinely examined in 1-5 dpf larvae using
462 fluorescent reporter lines and *in situ* RNA hybridization were HSPCs, neutrophils,
463 macrophages, erythrocytes, thrombocytes, rag+ T cells, and most recently eosinophils[60].
464 Others have detected gene expression in larvae characteristic of NK and ILC cells via
465 bulk methods like RT-PCR[61], but advancement in sequencing, combined with the
466 unbiased lineage tracing approach we took, allowed for detection of numerous new cell
467 types with improved precision and development of new RNA probes for cell type detection
468 *in situ*.

469 Two other scRNA-seq studies identified ILCs in the intestines and thymus of adult
470 zebrafish[24,35,62]. The top marker genes of intestinal ILC3s align with those detected at
471 larval stages, including *nitr* genes, *tnfa*, and *il17a/f3*[35,62]. Thymic ILC2s detected in
472 juveniles also express similar marker genes to those we observed in larvae including *il13*,
473 *il4*, *gata3*, and *si:dkey-21e2.10*[24]. The marker gene *eomesa* of the ILC1/NK-like
474 population was also detected in adult thymus NK-like cells using scRNA-seq[24]. There
475 remains some ambiguity on the absolute identity of some of cell types we identified as
476 the cells within some clusters have mixed identities. For example, in our assessment of
477 wildtype larvae, ILC3-like cells are found intermixed with il2rb+Tcells, but upon loss of
478 *rag1*, the populations become distinct. Similarly, ILC2-like cells are intermingled in a
479 single cluster in unperturbed conditions but become separated into two populations upon
480 loss of *rag1* and R848 treatment. Long-term lineage tracing studies are needed to clarify
481 how the newly identified larval populations separate and distribute among adult organ
482 system.

483 Much remains unknown about the regulation and function of the larval ILCs. Many
484 of the top marker genes in ILC populations remain uncharacterized. For example, the
485 ILC2 gene *swift* (aka *si:dkey-21e2.16*) is unannotated but has homology with granzyme
486 and chymase, which are more characteristic of cytotoxic immune cells like mast cells. A
487 recent study in humans showed that ILC2s express granzyme[63], indicating that ILC2s
488 may have more cytotoxic functions than previously appreciated. This finding hints at how
489 the unknown genes identified in the new immune effector cell clusters could reveal novel
490 biology of these lymphocytes. Moreover, the highly expressed and cell-type-restricted
491 marker genes for ILCs can be exploited to generate new transgenic lines to visualize how
492 larval and adult ILC populations shape organogenesis, immune responses, and diseases.
493 We also illustrated that larval ILCs have genetic dependencies consistent with their
494 innate lymphoid identity. We showed that ILCs expressing *eomesa, swift,* and *il7r* depend
495 on the functions of Il2rga and are independent of Rag1, consistent with murine studies[46].
496 Beyond ILCs, we uncovered novel Rag1-independent cells characterized by *blnk* and
497 *cd59* expression although their mammalian counterparts are unclear. To our knowledge,
498 this study is the first demonstration of the requirement for Runx1 for ILC development. As
499 we performed whole body loss-of-function studies, it is unclear if Runx1 is required
500 specifically within the stem and progenitor cells giving rise to the newly described
501 lymphoid populations or intrinsically within the mature cells. Factors like Runx1 show dual
502 requirements during the genesis of the definitive hematopoietic wave and within
503 differentiated immune effectors such as neutrophils and in megakaryocytes[38,64,65]. More
504 work is needed to identify if ILCs in zebrafish also require factors like *Eomes*, *Id2, Tcf7,*
505 *Gata3, Tox* and *Zbtb16* shown to be essential for development in other models[20]. Further
506 manipulation of the genes within each ILC cluster can uncover mechanisms controlling
507 the genesis of ILC lineages as well as the keys to their tissue distribution and functionality.
508 In general, ILCs participate in the immune responses to various pathogens like
509 bacteria, viruses, fungi, and helminths. Concordant with prior work, we showed that
510 ssRNA viral mimicry with the TLR7/8 agonist R848 expanded NK/ILC1-like cells[52]. Our
511 sequencing results showed a decrease in ILC2-like cells with R848 treatment, however
512 *in situ* hybridization did not recapitulate the result. We speculate that a portion of ILC2-

513 like cells may be dying in response to R848 and therefore are removed during cell sorting
514 prior to sequencing, while *in situ* hybridization may be capturing ILC2-like cells during the
515 process of dying. Lastly, R848 agonist also caused an expansion of T lymphocytes
516 although they appear to lack expression of the targeted Tlr7/8 receptors in our datasets.
517 It is possible that like in other model systems, interferon secreted by NK-cells recruits the
518 adaptive T lymphocytes via antigen presenting cells[66]. Further studies are needed to
519 determine if the mechanistic interplay between the immune cells is conserved in
520 zebrafish.

521 In summary, we identified how HSPCs differentiate to myeloid and lymphoid
522 lineages, including the previously unidentified larval ILCs in zebrafish. Studies on
523 mammalian adult ILCs are often complicated by the presence of T-helper cells which
524 closely resemble ILCs, so experiments are often done in a *Rag1/2* mutant context where
525 T lymphocytes are depleted. The zebrafish larval stage may be a unique time window for
526 studying ILCs in a non-perturbed, non-mutant context, pending further confirmation that
527 T-helper cell diversification to Th1, Th2, Th17 occurs later in zebrafish life. The discovery
528 of a wider variety of immune cells in larvae will permit the use of zebrafish for studying a
529 broader range of questions in the fields of immunology and disease.

530

531 **Limitations of the study**

532 We chose to use the *(drl:creER^{T2})* transgene based lineage tracing assay, because it is
533 established that it labels all cells within the adult kidney marrow[67]. Not all definitive
534 immune effectors derive from marrow hematopoiesis. Tissue-resident macrophages and
535 ILCs can seed peripheral organs independent of marrow hematopoiesis. Although we
536 detected a wide variety of immune effectors including those in mucosal tissues, it is
537 possible that the *(drl:creER^{T2})* system does not capture all HSPC subsets generating all
538 hematopoietic cells so we could be under sampling the immune landscape in larval
539 zebrafish by this labeling method.

540

541 **Acknowledgements**

542 T.V.B. was supported by grants from the National Institutes of Health (NIH)
543 R01DK121738, R01DK131445, R01DK141169, and the Edward P. Evans Foundation.
544 AN was supported by NIH F31HL167600, NYSTEM award C34874GG (PI Frenette), and
545 a Liang Zhu Memorial Fellowship. BAU was supported by NIH F31HL152562 and
546 T32GM007288 (PI Akabas), KJ was supported by T32GM145438 (PI Query) and
547 R01HL153920 (PI Zheng). Instrumental feedback to the development of this project was
548 provided by Dr. Kira Gritsman, Dr. Ulrich Steidl, and Dr. Meelad Dawlady. We thank the
549 Langenau lab for sharing *il2rga*^{Y91fs} mutant lines generated as part of R24OD016761. We
550 thank the core facilities instrumental for this work that are supported by the Einstein
551 National Cancer Institute's grant number P30CA013330, including: Flow Cytometry Core
552 Facility at Einstein and core members Yu (Joey) Zhang and Ming Liu for assistance with
553 FACS; the Einstein Genomics Core and core member David Reynolds for scRNA library
554 preparation; the Analytical Imaging Facility. We thank Dr. Roshan Sharma for meaningful
555 feedback on scRNA-seq data and Dr. Eliseo Castillo and Dr. Keir Balla for fruitful
556 discussions on innate lymphoid cells. Thank you to Dr. Noura Ghazale for meaningful
557 discussions and technical assistance, and Dr. Kathryn Potts for meaningful review and
558 discussion of the manuscript. Graphics were created in BioRender with copyright
559 https://BioRender.com/rsdc34d and https://BioRender.com/riwx66c
560

561 **Author Contributions**

562 Conceptualization, TVB, AN, BAU; Methodology, TVB, AN, BAU, KJ, DZ; Investigation,
563 TVB, AN, BAU; Writing—Original Draft, TVB, AN; Writing—Review & Editing, TVB, AN,
564 BAU, KJ, DZ; Funding Acquisition, TVB, AN; Supervision, DZ, TVB.
565

566 **Declaration of Interests**

567 The authors declare no competing interests.
568

569 **MATERIALS AND METHODS**

570 **KEY RESOURCES TABLE**

REAGENT or RESOURCE	SOURCE	IDENTIFIER

Antibodies		
Anti-Digoxigenin-AP (Anti-DIG)	Sigma	11093274910
Chemicals, peptides, and recombinant proteins		
(Z)-4-Hydroxytamoxifen	Sigma	H7904
4'6-Diamidino-2-phenlyindole (DAPI)	Sigma	D8417
R848 (Resiquimod)	InvivoGen	tlrl-r848-1
Liberase TM Research Grade	Sigma	5401127001
NBT/BCIP Color Development Substrate	Fisher	PR-S3771
Proteinase K, recombinant, PCR Grade	Sigma	3115887001
T7 Endonuclease I	NEB	M0302L
Alt-R™ S.p. Cas9 Nuclease V3	IDT	1081058
T7 RNA Polymerase	Sigma	10881775001
T3 RNA Polymerase	Sigma	11031163001
DIG RNA Labeling Mix	Sigma	11277073910
Deposited data		
Raw and processed scRNA-seq data	This paper	NCBI Accession: GSE292726
Experimental models: Organisms/strains		
Zebrafish *Tg(drl:CreER^{T2})*	Mosimann et al., 2015[23]	ZDB-TGCONSTRCT-160129-2
Zebrafish *Tg(ubi:loxP-GFP-loxP-stop-mCherry)*	Mosimann et al., 2011[22]	ZDB-ALT-110124-1
Zebrafish *Tg(rag2:mCherry)*	Harrold et al., 2016[68]	ZDB-TGCONSTRCT-160329-2
Zebrafish *runx1^{W84X}*	Jin et al., 2009[41]	ZDB-ALT-091019-1
Zebrafish *il2rga^{Y91fs}*	Tang et al., 2017[47]	ZDB-ALT-170710-3
Zebrafish AB (wild type)	ZIRC	ZL1
Oligonucleotides		
Alt-R® CRISPR-Cas9 tracrRNA	IDT	1072532
rag1 sgRNA #1: GGACTGCTGCCATAAGGGGA	ZFIN	ZDB-CRISPR-201209-4
rag1 sgRNA #2: AATGATGCCCACATCCCAGG	This paper	NA
rag1 sgRNA #3: TGACCGGCAAGTAACCATCA	This paper	NA
slc24a5 sgRNA: GGACAGACGTGTTTCTCCAG	Avagyan et al., 2021[69]	NA
Primer1 for *il7r* RNA probe: TAATACGACTCACTATAGGGGGCCTTCCTTTCACTTTCAG	This paper	NA
Primer2 for *il7r* RNA probe: CATTAACCCTCACTAAAGGGAACATGGATTAATGTCTATAGCAGAGGA	This paper	NA
SNP probe for *runx1^{W84X}* target sequence: GGTTCTGGTACCTTGAAGGCGATGGGCAGGGTCTTGTTGCAGCG[C/T]CAGTGTGTCGGCAGGACGGAGCAGAGGAAGTTCGGGCTGTCGG	Life Technologies	TaqMan® SNP Genotyping Assays
Recombinant DNA		

TCRalpha-L1 plasmid	Danilova et al., 2004[70]	Addgene Plasmid #11262
pTWIST-Kan-HighCopy-v2-eomesa plasmid	This paper	Addgene Plasmid #236391
pTWIST-Kan-HighCopy-v2-swift plasmid	This paper	Addgene Plasmid #236392
pENTR™5'-il7r plasmid	This paper	Addgene Plasmid #236393
Software and algorithms		
Cell Ranger v8.0.1 and v7.0.1	10XGenomics	https://support.10xgenomics.com/
Seurat 5.2	Hao et al., 2024[25]	https://satijalab.org/seurat/
clusterProfiler: enrichGO	Yu et al., 2012[71]	DOI: 10.18129/B9.bioc.clusterProfiler
Image Analysis: Fiji	Schindelin et al., 2012[72]	doi:10.1038/nmeth.2019
Photoshop CC 2022	Adobe	https://www.adobe.com/
Adobe Illustrator CC 2022	Adobe	https://www.adobe.com/
GraphPad Prism version 10.2.3	GraphPad	https://www.graphpad.com/
Other		
Resource website for scRNA-seq atlas	This paper	https://sites.google.com/view/tvbowmanlab/developmental-hematopoiesis-atlas

RESOURSE AVAILABILITY

Lead Contact

Further information and requests for resources, reagents, and other supporting data should be made to the Lead Contact, Teresa Bowman at teresa.bowman@einsteinmed.edu

Materials Availability

Reagents used in this study will be made available upon request. Plasmids for making RNA probes are deposited at Addgene.

Data and Code Availability

The sequencing data is available via the GEO accession number: GSE292726

584 The processed data can be viewed at:
585 https://sites.google.com/view/tvbowmanlab/developmental-hematopoiesis-atlas
586 Codes can be made available upon request.
587
588 **METHOD DETAILS**
589 **Zebrafish Husbandry**
590 Zebrafish were bred and maintained as described previously[73]. All fish were maintained
591 according to Institutional Animal Care and Use Committee (IACUC)-approved protocols
592 in accordance with the Albert Einstein College of Medicine research guidelines.
593
594 **Transgenic and Mutant Lines**
595 For lineage tracing, we used *Tg(drl:creER^{T2})* and the *Tg(ubi:loxP-GFP-loxP-stop-*
596 *mCherry)* also known as *Tg(ubi:Switch)*[22,23]. For all experiments, we crossed fish with two
597 copies of *Tg(drl:creER^{T2},ubi:Siwtch)* transgenes and crossed to WT AB fish so all
598 experimental animals were hemizygous. We used the published *runx1^{W84X}* mutants and
599 *il2rga^{Y91fs}* mutants[41,47]. Genotyping of *runx1^{W84X}* mutants was done using a SNP probe
600 and qPCR, and *il2rga^{Y91fs}* genotyping was done as described in Tang et.al[47]. To validate
601 the functional consequences of *rag1* crispants on T-cells, we used the
602 *Tg(rag2:mCherry)*[68].
603
604 **Lineage Tracing Assay**
605 To induce fluorescent-based lineage tracing of HSPCs, embryos containing
606 *Tg(drl:creER^{T2},ubi:Siwtch)* were incubated in a 28°C incubator with 12 μM 4-
607 hydroxytamoxifen for 20 hours, starting at 30 hpf for early HSPCs, at 54 hpf for mid
608 HSPCs, and at 86 hpf for late HSPCs. Hydroxytamoxifen was washed out three times
609 with embryo water then larvae were kept in clean dishes until endpoint.
610
611 **Single Cell RNA Sequencing**
612 *Cell isolation and Library Preparation*

613 For the early-HSPCs and mid-HSPCs cohorts, 200-250 larvae were used at one-day-post
614 labelling, 6 dpf, and 10 dpf. To obtain enough fluorescent cells from the late-HSPCs
615 derived cohort at the three timepoints 4, 6, and 10 dpf, we processed 1,100, 200, and 170
616 zebrafish larvae, respectively. For the *runx1*^{W84X} mutant experiment, 14 larvae were
617 processed for each condition. Homozygous *runx1* mutants were identified prior to
618 sequencing by scoring for absence of thymic mCherry signal and morphologically
619 observable thymic involution. Genotype was confirmed post-processing using left over
620 cells (data not shown). For the *rag1* crispants/R848 experiment, 35 larvae were
621 processed per condition. For processing of all samples, whole larvae were minced with a
622 razor blade and digested with 5 mg/mL liberase for 15 minutes at 37°C, followed by FBS
623 inactivation as previously described[14]. The mCherry-expressing cells were sorted out
624 using the BD FACSAria II machine into buffer made of 500 μL IMDM + 10% FBS at room
625 temperature machine setting. The cells were immediately processed for cell capture by
626 the Einstein genomics facility, using the "Chromium Next GEM Single Cell 3′ Kit v3.1" for
627 samples in Figures 1-5 and the "Chromium Next GEM Single Cell 3′ Kit v4" kit for *rag1*
628 crispant/R848 samples in Figures 6 & 7. Cell numbers for each experiment are listed in
629 Tables S1-7.
630
631 *Quality Control and Analysis*
632 Fastq files for *rag1* crispant/R848 experiment were processed in Cell Ranger 8.0.1 using
633 the count function and all other experiments were processed in Cell Ranger 7.0.1. To
634 generate the counts matrix in Cell Ranger, we made a custom reference genome based
635 on *Danio rerio* GRCz11 with the addition of mCherry, and T cell specific genes: TCRaC,
636 TCRbC1 and TCRbC2. All subsequent analysis was done in Seurat version 5.2.0[25]. No
637 batch effect was apparent between samples, so all analysis was done without batch
638 corrections **(Figure S1D, S2E).** For all experiments, cells with less than 200 genes and
639 more than 10% mitochondrial DNA were filtered out **(Figure S1, S2, S4, S5)**. For the
640 lineage tracing dataset in Figure 1, we used the 4,000 top variable features for initial
641 dimensional reduction, with 30 principal components (PC) and at cluster resolution of 1.
642 After non-hematopoietic cells were removed, the remaining hematopoietic cells were re-

643 analyzed with top 2,000 variable features, 30 PCs and at cluster resolution of 1 **(Figure**
644 **S1A,F)**. Two more lower quality clusters were identified and removed to obtain the final
645 clustering using 2,000 variable features, 20 PCs, and cluster resolution of 1. For the
646 lymphoid only subset analysis in Figure 4A, we used 2,000 variable genes, 25 PCs, and
647 0.3 cluster resolution. For the *runx1* mutant dataset in Figure 5, we included a wild-type
648 control dataset at 6 dpf derived from the early-HSPCs trace to check for common
649 identification of clusters between experiments. For initial clustering we used 4,000
650 variable genes, 30 PCs, and cluster resolution of 1. We removed non-hematopoietic
651 clusters based on top marker genes, and the final dataset was generated using 2,000
652 variable genes, with 20 PCs, and at a cluster resolution of 0.7. For *rag1* crispant/R848
653 dataset in Figures 6-7, initial clustering was done using 4,000 variable genes, 30 PCs,
654 and cluster resolution of 1. After removing non-hematopoietic cells, final clustering was
655 done using 2,000 variable genes, 20 PCs, and a cluster resolution of 1. For analysis of
656 the lymphoid only subset, we used 1,000 variable genes, 15 PCs, and 0.2 cluster
657 resolution. Cluster identities were assigned based on literature and top marker genes
658 obtained using the FindAllMarkers function in Seurat which compares the target cluster
659 to other clusters using the Wilcoxon Rank Sum test.
660
661 *Differential Expression and GO Enrichment Analysis*
662 For differential gene expression analysis, two clusters of interest were compared using
663 the FindMarkers function in Seurat using standard settings for Wilcoxon Rank Sum test.
664 For gene enrichment analysis, the list of genes obtained from differential expression
665 analysis was filtered to include only those with adjusted p-value of less that 0.05, and an
666 average fold-change greater than 1.5. Using the enrichGO function available in
667 ClusterProfiler package, we identified overrepresented GO terms that belong to the
668 Biological Processes category. Displayed in the Figures 2E, 3C', and S6D are selected
669 GO categories from the output list.
670
671 *Pseudotime Analysis*

672 The software Psupertime[29] was used to temporally order each cluster of cells in the
673 hematopoietic atlas dataset from the different lineage traces. We include in the
674 supplement results from psupertime on two clusters of cells identified as macrophages
675 and neutrophils (Figure S3). Psupertime was run with default settings with the exception
676 of "min_expression" set to 0.00 instead of 0.01 to include genes that were expressed in
677 any cell rather than at least 1% to ensure that rare lineage genes were not missed due to
678 low abundance of some cell types in some traces.
679
680 **Confocal Microscopy and Analysis**
681 The CSU-W1 Nikon spinning disc confocal was used for all high-resolution imaging of
682 lineage tracing in wild-type and mutant conditions and in drug-treated larvae. For live
683 imaging, larvae were anesthetized with 0.01% tricaine and mounted in 4%
684 methylcellulose on glass bottom dished. Images were acquired using 10x lens with the
685 following parameters: 600 millisecond exposure, and 561λ laser at 65% power and the z-
686 stack was set to 6 μm size steps. Images were analyzed in Fiji (ImageJ) version 2.1.0. To
687 calculate mCherry signal in the thymus and CHT, we used Corrected Total Cell
688 Fluorescence formular: (Integrated density of region of interest) - (Area of region of
689 interest x Mean fluorescence of 6 different background regions). All quantification of live
690 imaging was done blindly to genotype and/or condition, with the exception of images in
691 Figure 2F and Figure 3A.
692
693 ***In situ* Hybridization**
694 The *tcra* RNA probe was made from Addgene plasmid #11262 gifted by Lisa Steiner[70].
695 The *il7r* RNA probe was made off a PCR template that was amplified from cDNA collected
696 from 10 dpf whole larvae. Transcription of the anti-sense *il7r* RNA off the PCR template
697 was done using T3 RNA polymerase. To make *eomesa* and *swift* probes, the DNA
698 sequences were synthesized and put into pTWIST-kan high copy vector by TWIST
699 Bioscience. For *eomesa* probe, a 971 bp fragment containing exon 7 - 3'UTR region and
700 flanked by T7 and T3 primers was synthesized. For *swift* probe, a 922 bp fragment was
701 made containing the entire coding region of the gene. Gene-specific primers that

702 contained T3 RNA polymerase sequence (forward) and T7 RNA polymerase sequence
703 (reverse) at the 5'end were then used to generate a linear PCR-amplified template for *in*
704 *vitro* transcription using T7 RNA polymerase. Whole mount *in situ* RNA hybridization was
705 done based on established zebrafish protocols with modifications for older larvae[74]. For
706 6 & 8 dpf stages, pigment was removed by bleaching with a solution of 0.8%KOH, 0.9%
707 H_2O_2, and 0.1% Tween20 for 35 & 45 min, respectively. Proteinase K working
708 concentration was increased to 15 mg/mL, and digestion time was extended to 35 & 40
709 min for 6 & 8 dpf, respectively. After digestion, samples were fixed with 0.25%
710 glutaraldehyde for 25 and 30 minutes for 6 & 8 dpf, respectively. Incubation in RNA probes
711 was done for two nights at 70°C to maximize detection. To visualize the RNA probe signal,
712 we used anti-DIG followed by colorimetric detection using NBT/BCIP. Samples were
713 incubated in NBT/BCIP for 1-3 days for *eomesa* or *il7r*, and 8 hours for *swift,* all at room
714 temperature. For experiments with *runx1*^{W84X} and *il2rga*^{Y91fs} mutants, each embryo was
715 imaged, quantified, and then genotyped. All quantification was done blindly to genotype
716 and condition, except for experiments in Figure 6C and 7E for *eomesa* and *il7r* probes.
717 Full images of *swift* expression are shown in the supplemental figures.
718

719 **CRISPR/Cas9 Mutagenesis**

720 The crispant approach was used to mutagenize the *rag1* locus, where a single guide RNA
721 and Cas9 protein were assembled into a complex and injected into one-cell stage
722 embryos[75]. The single guide RNA was assembled by annealing a tracr RNA with the locus
723 specific crRNA for 5 min at 95°C, and cooled at room temperature for 10 min. Three
724 guides were used to target the *rag1* locus, two of them were designed in CHOPCHOP,
725 and one sequence that is deposited in ZFIN **(Figure S5)**[76]. As a control for mutagenesis,
726 the *slc26a4* (golden) guide RNA was used[69]. Each single guide RNA was assembled into
727 a complex with Cas9 separately. For the control, *slc24a5* targeting complex alone was
728 injected, and for *rag1* crispants, the four guide complexes (3 *rag1* guides + 1 *slc24a5*
729 guide) were mixed in equal volumes. A T7 endonuclease assay was used to confirm
730 mutagenesis, where a cutting occurs only in the presence of heteroduplex DNA indicating
731 mutagenesis **(Figure S5)**.

732

733 **Resiquimod R848 Drug Treatment**

734 The 500 μg of R848 powder was obtained from InvivoGen and reconstituted in 500 μL of
735 water for a final concentration of 1 μg/μL or 2.85 mM. To treat larvae, the stock was diluted
736 in embryo water to a working concentration of 28.5 μM. Larvae were incubated with R848
737 starting at 6 dpf and analyzed at 8 dpf.

738

739 **Statistical Analysis**

740 Analysis was done in GraphPad Prism 10.2.3. For all experiments with 3 groups, a one-
741 way ANOVA with Tukey multiple testing corrections was used. For 2 groups, an unpaired
742 t-test was used as indicated in the figure legends. All error bars show standard deviation
743 from the mean. A Chi-square test was used to compare number of cells per cluster in the
744 stacked bar plots. In all plots, one point is a single zebrafish larva. For single-cell RNA
745 sequencing, one replicate was done per condition. Confocal imaging experiments were
746 done with at least 3 independent experiments, and in situ experiments were done at least
747 2 independent times. In all figures: ns = not significant, * = $p< 0.05$, ** = $p<0.01$, *** =
748 $p<0.001$, **** = $p<0.0001$.

749

750 **REFERENCES**

751

752 1 Gore, A. V., Pillay, L. M., Venero Galanternik, M. & Weinstein, B. M. The
753 zebrafish: A fintastic model for hematopoietic development and disease. *Wiley*
754 *Interdiscip Rev Dev Biol* **7**, e312, doi:10.1002/wdev.312 (2018).

755 2 Kobayashi, M. & Yoshimoto, M. Multiple waves of fetal-derived immune cells
756 constitute adult immune system. *Immunol Rev* **315**, 11-30,
757 doi:10.1111/imr.13192 (2023).

758 3 Jagannathan-Bogdan, M. & Zon, L. I. Hematopoiesis. *Development* **140**, 2463-
759 2467, doi:10.1242/dev.083147 (2013).

760 4 McGrath, K. E., Frame, J. M. & Palis, J. Early hematopoiesis and macrophage
761 development. *Semin Immunol* **27**, 379-387, doi:10.1016/j.smim.2016.03.013
762 (2015).

763 5 Le Guyader, D. *et al.* Origins and unconventional behavior of neutrophils in
764 developing zebrafish. *Blood* **111**, 132-141, doi:10.1182/blood-2007-06-095398
765 (2008).

766 6 Canu, G. & Ruhrberg, C. First blood: the endothelial origins of hematopoietic
767 progenitors. *Angiogenesis* **24**, 199-211, doi:10.1007/s10456-021-09783-9 (2021).

768 7 Dege, C. *et al.* Potently Cytotoxic Natural Killer Cells Initially Emerge from
769 Erythro-Myeloid Progenitors during Mammalian Development. *Dev Cell* **53**, 229-
770 239 e227, doi:10.1016/j.devcel.2020.02.016 (2020).

771 8 Kissa, K. & Herbomel, P. Blood stem cells emerge from aortic endothelium by a
772 novel type of cell transition. *Nature* **464**, 112-115, doi:10.1038/nature08761
773 (2010).

774 9 Bertrand, J. Y. *et al.* Haematopoietic stem cells derive directly from aortic
775 endothelium during development. *Nature* **464**, 108-111, doi:10.1038/nature08738
776 (2010).

777 10 Murayama, E. *et al.* Tracing hematopoietic precursor migration to successive
778 hematopoietic organs during zebrafish development. *Immunity* **25**, 963-975,
779 doi:10.1016/j.immuni.2006.10.015 (2006).

780 11 Chen, M. J. *et al.* Erythroid/myeloid progenitors and hematopoietic stem cells
781 originate from distinct populations of endothelial cells. *Cell Stem Cell* **9**, 541-552,
782 doi:10.1016/j.stem.2011.10.003 (2011).

783 12 Dignum, T. *et al.* Multipotent progenitors and hematopoietic stem cells arise
784 independently from hemogenic endothelium in the mouse embryo. *Cell Rep* **36**,
785 109675, doi:10.1016/j.celrep.2021.109675 (2021).

786 13 Ghersi, J. J. *et al.* Haematopoietic stem and progenitor cell heterogeneity is
787 inherited from the embryonic endothelium. *Nat Cell Biol* **25**, 1135-1145,
788 doi:10.1038/s41556-023-01187-9 (2023).

789 14 Ulloa, B. A. *et al.* Definitive hematopoietic stem cells minimally contribute to
790 embryonic hematopoiesis. *Cell Rep* **36**, 109703,
791 doi:10.1016/j.celrep.2021.109703 (2021).

792 15 Tian, Y. *et al.* The first wave of T lymphopoiesis in zebrafish arises from aorta
793 endothelium independent of hematopoietic stem cells. *J Exp Med* **214**, 3347-
794 3360, doi:10.1084/jem.20170488 (2017).

795 16 He, S. *et al.* In vivo single-cell lineage tracing in zebrafish using high-resolution
796 infrared laser-mediated gene induction microscopy. *Elife* **9**,
797 doi:10.7554/eLife.52024 (2020).

798 17 Neo, W. H., Lie, A. L. M., Fadlullah, M. Z. H. & Lacaud, G. Contributions of
799 Embryonic HSC-Independent Hematopoiesis to Organogenesis and the Adult
800 Hematopoietic System. *Front Cell Dev Biol* **9**, 631699,
801 doi:10.3389/fcell.2021.631699 (2021).

802 18 Cherrier, D. E., Serafini, N. & Di Santo, J. P. Innate Lymphoid Cell Development:
803 A T Cell Perspective. *Immunity* **48**, 1091-1103,
804 doi:10.1016/j.immuni.2018.05.010 (2018).

805 19 Spits, H. *et al.* Innate lymphoid cells--a proposal for uniform nomenclature. *Nat*
806 *Rev Immunol* **13**, 145-149, doi:10.1038/nri3365 (2013).

807 20 Klose, C. S. N. & Artis, D. Innate lymphoid cells control signaling circuits to
808 regulate tissue-specific immunity. *Cell Res* **30**, 475-491, doi:10.1038/s41422-
809 020-0323-8 (2020).

810 21 Yuan, T. *et al.* Innate lymphoid cells and infectious diseases. *Innate Immun* **30**,
811 120-135, doi:10.1177/17534259241287311 (2024).

812 22 Mosimann, C. *et al.* Ubiquitous transgene expression and Cre-based
813 recombination driven by the ubiquitin promoter in zebrafish. *Development* **138**,
814 169-177, doi:10.1242/dev.059345 (2011).

815 23 Mosimann, C. *et al.* Chamber identity programs drive early functional partitioning
816 of the heart. *Nat Commun* **6**, 8146, doi:10.1038/ncomms9146 (2015).

817 24 Rubin, S. A. *et al.* Single-cell analyses reveal early thymic progenitors and pre-B
818 cells in zebrafish. *J Exp Med* **219**, doi:10.1084/jem.20220038 (2022).

819 25 Hao, Y. *et al.* Dictionary learning for integrative, multimodal and scalable single-
820 cell analysis. *Nat Biotechnol* **42**, 293-304, doi:10.1038/s41587-023-01767-y
821 (2024).

822 26 Ouyang, J. F., Kamaraj, U. S., Cao, E. Y. & Rackham, O. J. L. ShinyCell: simple
823 and sharable visualization of single-cell gene expression data. *Bioinformatics* **37**,
824 3374-3376, doi:10.1093/bioinformatics/btab209 (2021).

825 27 Soza-Ried, C., Hess, I., Netuschil, N., Schorpp, M. & Boehm, T. Essential role of
826 c-myb in definitive hematopoiesis is evolutionarily conserved. *Proc Natl Acad Sci*
827 *U S A* **107**, 17304-17308, doi:10.1073/pnas.1004640107 (2010).

828 28 Gao, X., Xu, C., Asada, N. & Frenette, P. S. The hematopoietic stem cell niche:
829 from embryo to adult. *Development* **145**, doi:10.1242/dev.139691 (2018).

830 29 Macnair, W., Gupta, R. & Claassen, M. psupertime: supervised pseudotime
831 analysis for time-series single-cell RNA-seq data. *Bioinformatics* **38**, i290-i298,
832 doi:10.1093/bioinformatics/btac227 (2022).

833 30 Langenau, D. M. *et al.* In vivo tracking of T cell development, ablation, and
834 engraftment in transgenic zebrafish. *Proc Natl Acad Sci U S A* **101**, 7369-7374,
835 doi:10.1073/pnas.0402248101 (2004).

836 31 Langenau, D. M. & Zon, L. I. The zebrafish: a new model of T-cell and thymic
837 development. *Nat Rev Immunol* **5**, 307-317, doi:10.1038/nri1590 (2005).

838 32 Dorshkind, K. & Crooks, G. Layered immune system development in mice and
839 humans. *Immunol Rev* **315**, 5-10, doi:10.1111/imr.13198 (2023).

840 33 Tang, Y. *et al.* Emergence of NK-cell progenitors and functionally competent NK-
841 cell lineage subsets in the early mouse embryo. *Blood* **120**, 63-75,
842 doi:10.1182/blood-2011-02-337980 (2012).

843 34 Schneider, C. *et al.* Tissue-Resident Group 2 Innate Lymphoid Cells Differentiate
844 by Layered Ontogeny and In Situ Perinatal Priming. *Immunity* **50**, 1425-1438
845 e1425, doi:10.1016/j.immuni.2019.04.019 (2019).

846 35 Hernandez, P. P. *et al.* Single-cell transcriptional analysis reveals ILC-like cells in
847 zebrafish. *Sci Immunol* **3**, doi:10.1126/sciimmunol.aau5265 (2018).

848 36 Naito, M. & Kumanogoh, A. Group 2 innate lymphoid cells and their surrounding
849 environment. *Inflamm Regen* **43**, 21, doi:10.1186/s41232-023-00272-8 (2023).

850 37 Hernandez-Torres, D. C. & Stehle, C. Embryonic ILC-poiesis across tissues.
851 *Front Immunol* **13**, 1040624, doi:10.3389/fimmu.2022.1040624 (2022).

852 38 Yzaguirre, A. D., de Bruijn, M. F. & Speck, N. A. The Role of Runx1 in Embryonic
853 Blood Cell Formation. *Adv Exp Med Biol* **962**, 47-64, doi:10.1007/978-981-10-
854 3233-2_4 (2017).

855 39 Kalev-Zylinska, M. L. *et al.* Runx1 is required for zebrafish blood and vessel
856 development and expression of a human RUNX1-CBF2T1 transgene advances a
857 model for studies of leukemogenesis. *Development* **129**, 2015-2030,
858 doi:10.1242/dev.129.8.2015 (2002).

859 40 North, T. E. *et al.* Runx1 expression marks long-term repopulating hematopoietic
860 stem cells in the midgestation mouse embryo. *Immunity* **16**, 661-672,
861 doi:10.1016/s1074-7613(02)00296-0 (2002).

862 41 Jin, H. *et al.* Definitive hematopoietic stem/progenitor cells manifest distinct
863 differentiation output in the zebrafish VDA and PBI. *Development* **136**, 647-654,
864 doi:10.1242/dev.029637 (2009).

865 42 Sasaki, K. *et al.* Absence of fetal liver hematopoiesis in mice deficient in
866 transcriptional coactivator core binding factor beta. *Proc Natl Acad Sci U S A* **93**,
867 12359-12363, doi:10.1073/pnas.93.22.12359 (1996).

868 43 Wang, Q. *et al.* Disruption of the Cbfa2 gene causes necrosis and hemorrhaging
869 in the central nervous system and blocks definitive hematopoiesis. *Proc Natl*
870 *Acad Sci U S A* **93**, 3444-3449, doi:10.1073/pnas.93.8.3444 (1996).

871 44 Tober, J. *et al.* The megakaryocyte lineage originates from hemangioblast
872 precursors and is an integral component both of primitive and of definitive
873 hematopoiesis. *Blood* **109**, 1433-1441, doi:10.1182/blood-2006-06-031898
874 (2007).

875 45 Potts, K. S. *et al.* A lineage of diploid platelet-forming cells precedes polyploid
876 megakaryocyte formation in the mouse embryo. *Blood* **124**, 2725-2729,
877 doi:10.1182/blood-2014-02-559468 (2014).

878 46 Colonna, M. Innate Lymphoid Cells: Diversity, Plasticity, and Unique Functions in
879 Immunity. *Immunity* **48**, 1104-1117, doi:10.1016/j.immuni.2018.05.013 (2018).

880 47 Tang, Q. *et al.* Dissecting hematopoietic and renal cell heterogeneity in adult
881 zebrafish at single-cell resolution using RNA sequencing. *J Exp Med* **214**, 2875-
882 2887, doi:10.1084/jem.20170976 (2017).

883 48 Sertori, R. *et al.* Conserved IL-2Rgammac Signaling Mediates Lymphopoiesis in
884 Zebrafish. *J Immunol* **196**, 135-143, doi:10.4049/jimmunol.1403060 (2016).

885 49 Lamason, R. L. *et al.* SLC24A5, a putative cation exchanger, affects
886 pigmentation in zebrafish and humans. *Science* **310**, 1782-1786,
887 doi:10.1126/science.1116238 (2005).

888 50 Ver Heul, A. M. *et al.* RAG suppresses group 2 innate lymphoid cells. *bioRxiv*,
889 doi:10.1101/2024.04.23.590767 (2024).

890 51 Veneziani, I., Alicata, C., Moretta, L. & Maggi, E. Human toll-like receptor 8
891 (TLR8) in NK cells: Implication for cancer immunotherapy. *Immunol Lett* **261**, 13-
892 16, doi:10.1016/j.imlet.2023.07.003 (2023).

893 52 Veneziani, I. *et al.* Toll-like receptor 8 agonists improve NK-cell function primarily
894 targeting CD56(bright)CD16(-) subset. *J Immunother Cancer* **10**, doi:10.1136/jitc-
895 2021-003385 (2022).

896 53 Anfray, C. *et al.* Intratumoral combination therapy with poly(I:C) and resiquimod
897 synergistically triggers tumor-associated macrophages for effective systemic
898 antitumoral immunity. *J Immunother Cancer* **9**, doi:10.1136/jitc-2021-002408
899 (2021).

900 54 Lopez-Cuevas, P. *et al.* Reprogramming macrophages with R848-loaded artificial
901 protocells to modulate skin and skeletal wound healing. *J Cell Sci* **137**,
902 doi:10.1242/jcs.262202 (2024).

903 55 Zhou, J., Nouri-Shirazi, M., Tang, H., Shen, Y. & Zeng, M. R848/TLR7-Mediated
904 Stronger CD8+ T Immunity Is Dependent on DC-NK Cell Interactions. *Int Arch*
905 *Allergy Immunol* **183**, 860-875, doi:10.1159/000522364 (2022).

906 56 Okuzumi, S. *et al.* TLR7 Agonist Suppresses Group 2 Innate Lymphoid Cell-
907 mediated Inflammation via IL-27-Producing Interstitial Macrophages. *Am J Respir*
908 *Cell Mol Biol* **65**, 309-318, doi:10.1165/rcmb.2021-0042OC (2021).

909 57 Elsaid, R. *et al.* A wave of bipotent T/ILC-restricted progenitors shapes the
910 embryonic thymus microenvironment in a time-dependent manner. *Blood* **137**,
911 1024-1036, doi:10.1182/blood.2020006779 (2021).

912 58 Simic, M. *et al.* Distinct Waves from the Hemogenic Endothelium Give Rise to
913 Layered Lymphoid Tissue Inducer Cell Ontogeny. *Cell Rep* **32**, 108004,
914 doi:10.1016/j.celrep.2020.108004 (2020).

915 59 Garcia-Lopez, J. P. *et al.* Ontogenetically distinct neutrophils differ in function
916 and transcriptional profile in zebrafish. *Nat Commun* **14**, 4942,
917 doi:10.1038/s41467-023-40662-7 (2023).

918 60 Li, G. *et al.* Cebp1 and Cebpbeta transcriptional axis controls eosinophilopoiesis
919 in zebrafish. *Nat Commun* **15**, 811, doi:10.1038/s41467-024-45029-0 (2024).

920 61 Pereiro, P. *et al.* Zebrafish Nk-lysins: First insights about their cellular and
921 functional diversification. *Dev Comp Immunol* **51**, 148-159,
922 doi:10.1016/j.dci.2015.03.009 (2015).

923 62 Jones, L. O. *et al.* Single-cell resolution of the adult zebrafish intestine under
924 conventional conditions and in response to an acute Vibrio cholerae infection.
925 *Cell Rep* **42**, 113407, doi:10.1016/j.celrep.2023.113407 (2023).

926 63 Li, Z. *et al.* Therapeutic application of human type 2 innate lymphoid cells via
927 induction of granzyme B-mediated tumor cell death. *Cell* **187**, 624-641 e623,
928 doi:10.1016/j.cell.2023.12.015 (2024).

929 64 Huang, Z. *et al.* Runx1 regulates zebrafish neutrophil maturation via synergistic
930 interaction with c-Myb. *J Biol Chem* **296**, 100272, doi:10.1016/j.jbc.2021.100272
931 (2021).

932 65 Zezulin, A. U. *et al.* RUNX1 is required in granulocyte-monocyte progenitors to
933 attenuate inflammatory cytokine production by neutrophils. *Genes Dev* **37**, 605-
934 620, doi:10.1101/gad.350418.123 (2023).

935 66 Iwasaki, A. & Medzhitov, R. Toll-like receptor control of the adaptive immune
936 responses. *Nat Immunol* **5**, 987-995, doi:10.1038/ni1112 (2004).

937 67 Henninger, J. *et al.* Clonal fate mapping quantifies the number of haematopoietic
938 stem cells that arise during development. *Nat Cell Biol* **19**, 17-27,
939 doi:10.1038/ncb3444 (2017).

940 68 Harrold, I. *et al.* Efficient transgenesis mediated by pigmentation rescue in
941 zebrafish. *Biotechniques* **60**, 13-20, doi:10.2144/000114368 (2016).

942 69 Avagyan, S. *et al.* Resistance to inflammation underlies enhanced fitness in
943 clonal hematopoiesis. *Science* **374**, 768-772, doi:10.1126/science.aba9304
944 (2021).

945 70 Danilova, N. *et al.* T cells and the thymus in developing zebrafish. *Dev Comp*
946 *Immunol* **28**, 755-767, doi:10.1016/j.dci.2003.12.003 (2004).

947 71 Yu, G., Wang, L. G., Han, Y. & He, Q. Y. clusterProfiler: an R package for
948 comparing biological themes among gene clusters. *OMICS* **16**, 284-287,
949 doi:10.1089/omi.2011.0118 (2012).

950 72 Schindelin, J. *et al.* Fiji: an open-source platform for biological-image analysis.
951 *Nat Methods* **9**, 676-682, doi:10.1038/nmeth.2019 (2012).

952 73 Lawrence, C. in *Methods in Cell Biology* Vol. 104 (eds H. William Detrich, Monte
953 Westerfield, & Leonard I. Zon) 429-451 (Academic Press, 2011).

954 74 Thisse, C. & Thisse, B. High-resolution in situ hybridization to whole-mount
955 zebrafish embryos. *Nat Protoc* **3**, 59-69, doi:10.1038/nprot.2007.514 (2008).

956 75 Burger, A. *et al.* Maximizing mutagenesis with solubilized CRISPR-Cas9
957 ribonucleoprotein complexes. *Development* **143**, 2025-2037,
958 doi:10.1242/dev.134809 (2016).

959 76 Labun, K. *et al.* CHOPCHOP v3: expanding the CRISPR web toolbox beyond
960 genome editing. *Nucleic Acids Res* **47**, W171-W174, doi:10.1093/nar/gkz365
961 (2019).
962

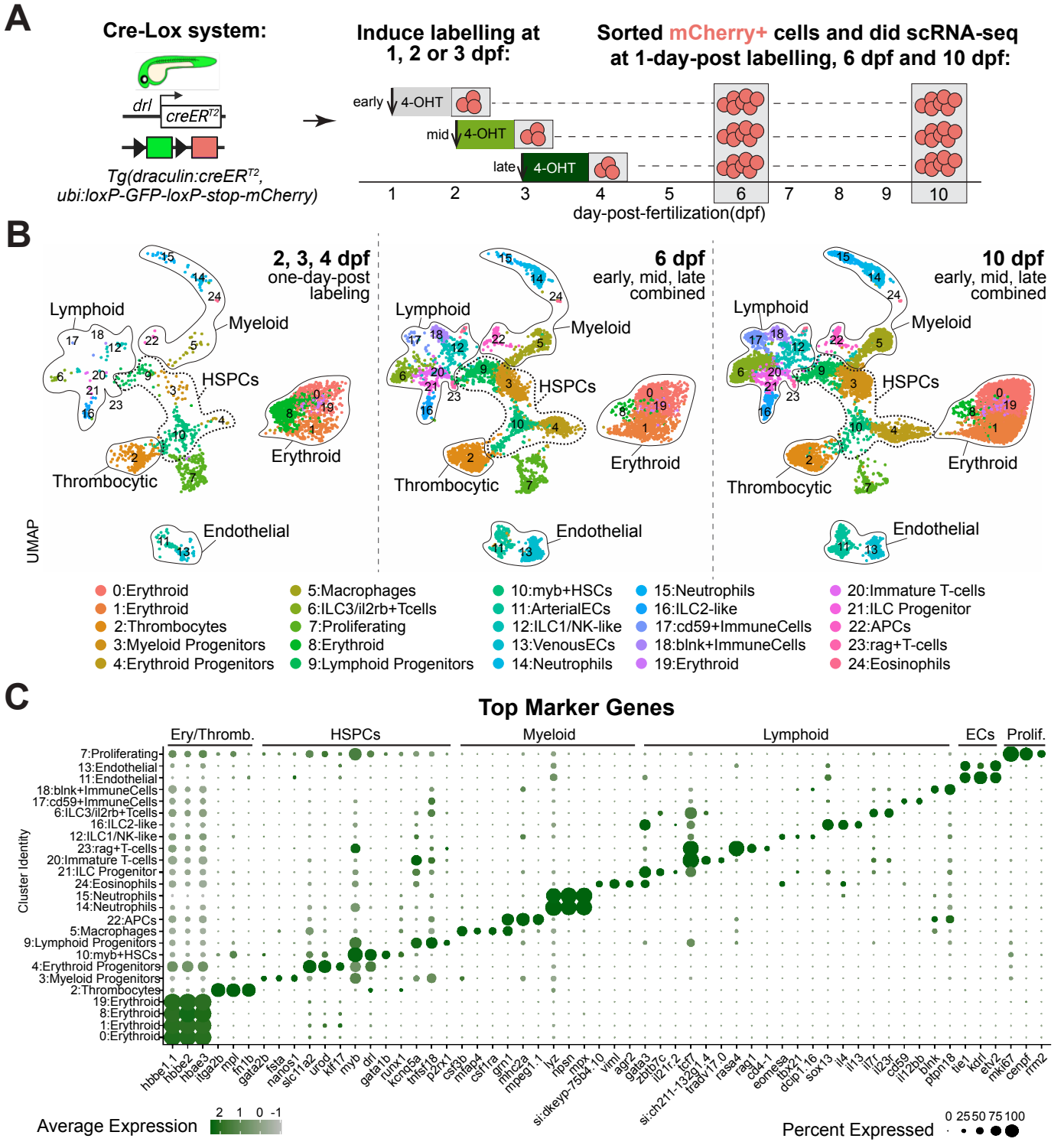

Figure 1. Single cell atlas of hematopoietic and immune cells detected during zebrafish development. (**A**) Hematopoietic-selective and tamoxifen-inducible Cre-Lox labelling system was activated by addition of 12 μM hydroxy-tamoxifen at either 1, 2, or 3 days-post-fertilization (dpf) which we termed the "early-HSPCs", "mid-HSPCs" and "late-HSPCs" respectively (2). The mCherry-expressing progeny of each trace was captured at three developmental timepoints using single cell RNA sequencing (scRNA-seq), at one-day-post labelling (1 dpl), 6 dpf, and at 10 dpf (3). (**B**) UMAP

showing clusters detected at 1 dpl, 6 dpf, and 10 dpf derived from any of the HSPC tracing paradigms. The dotted line highlights all HSPC populations including LyPs, MyPs, EryPs and HSCs, while solid lines highlight mature cells by lineage. (**C**) Dot plot displaying top marker genes of erythrocytes, thrombocytes, myelocytes, lymphocytes, stem & progenitor cells, endothelium, and proliferating cells that were obtained using the FindAllMarkers function in Seurat with Wilcoxon Rank Sum testing.

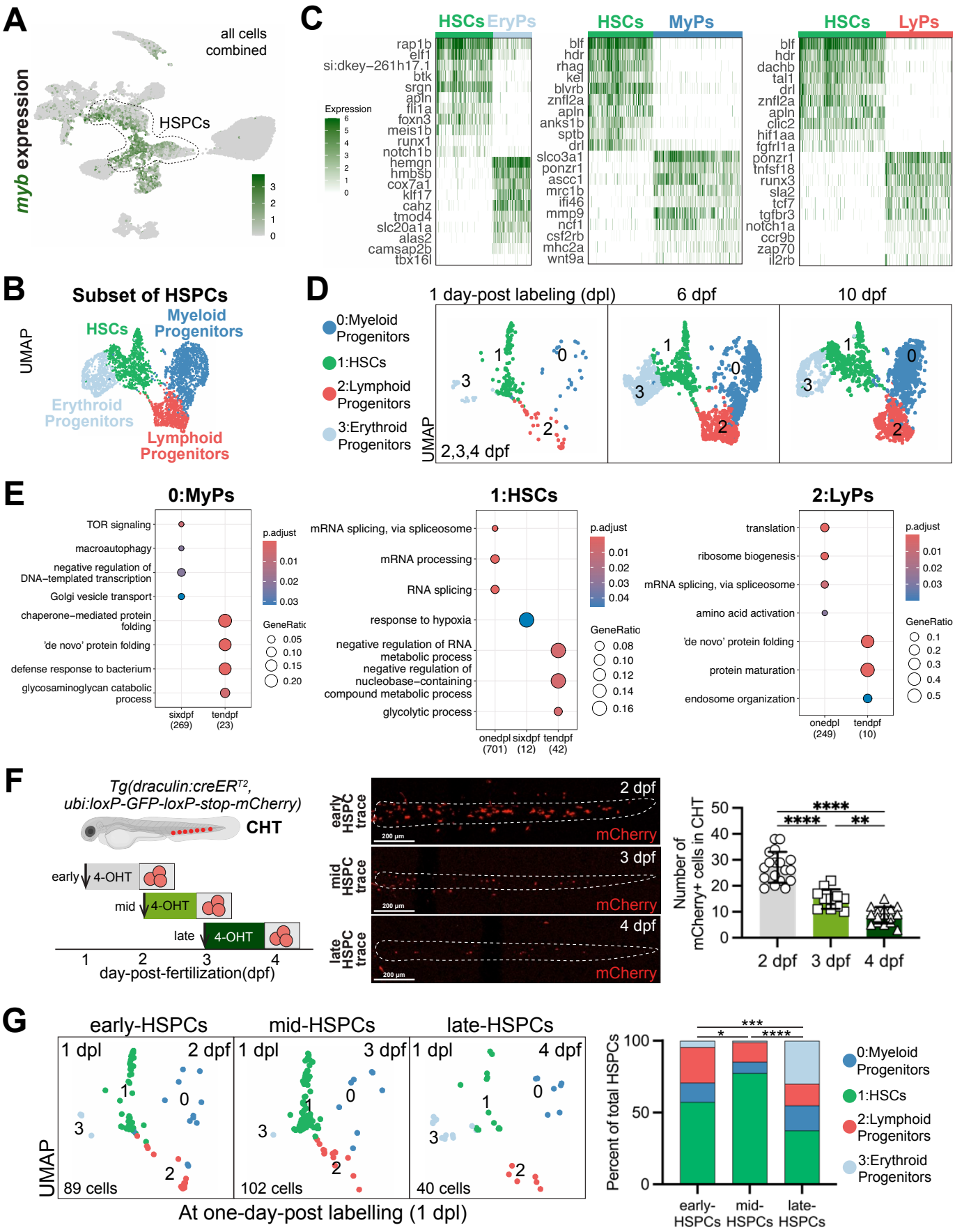
A
all cells combined
myb expression
HSPCs
C
HSCs EryPs
HSCs MyPs
HSCs LyPs
Expression
rap1b
elf1
si:dkey-261h17.1
btk
srgn
apln
fli1a
foxn3
meis1b
runx1
notch1b
hemgn
hmbsb
cox7a1
klf17
cahz
tmod4
slc20a1a
alas2
camsap2b
tbx16l
blf
hdr
rhag
kel
blvrb
znfl2a
apln
anks1b
sptb
drl
slco3a1
ponzr1
ascc1
mrc1b
ifi46
mmp9
ncf1
csf2rb
mhc2a
wnt9a
dachb
tal1
drl
znfl2a
apln
clic2
hif1aa
fgfrl1a
ponzr1
tnfsf18
runx3
sla2
tcf7
tgfbr3
notch1a
ccr9b
zap70
il2rb
B
Subset of HSPCs
UMAP
HSCs
Myeloid Progenitors
Erythroid Progenitors
Lymphoid Progenitors
D
1 day-post labeling (dpl)
6 dpf
10 dpf
0:Myeloid Progenitors
1:HSCs
2:Lymphoid Progenitors
3:Erythroid Progenitors
UMAP
2,3,4 dpf
E
0:MyPs
1:HSCs
2:LyPs
TOR signaling
macroautophagy
negative regulation of DNA-templated transcription
Golgi vesicle transport
chaperone-mediated protein folding
'de novo' protein folding
defense response to bacterium
glycosaminoglycan catabolic process
sixdpf (269)
tendpf (23)
p.adjust
GeneRatio
mRNA splicing, via spliceosome
mRNA processing
RNA splicing
response to hypoxia
negative regulation of RNA metabolic process
negative regulation of nucleobase-containing compound metabolic process
glycolytic process
onedpl (701)
sixdpf (12)
tendpf (42)
translation
ribosome biogenesis
mRNA splicing, via spliceosome
amino acid activation
'de novo' protein folding
protein maturation
endosome organization
onedpl (249)
tendpf (10)
F
Tg(draculin:creER^{T2}, ubi:loxP-GFP-loxP-stop-mCherry)
CHT
early 4-OHT
mid 4-OHT
late 4-OHT
day-post-fertilization(dpf)
early HSPC trace
mid HSPC trace
late HSPC trace
2 dpf
3 dpf
4 dpf
mCherry
200 µm
Number of mCherry+ cells in CHT
G
early-HSPCs
mid-HSPCs
late-HSPCs
1 dpl
2 dpf
3 dpf
4 dpf
UMAP
89 cells
102 cells
40 cells
At one-day-post labelling (1 dpl)
Percent of total HSPCs
early-HSPCs
mid-HSPCs
late-HSPCs
0:Myeloid Progenitors
1:HSCs
2:Lymphoid Progenitors
3:Erythroid Progenitors

Figure 2. Comparison of contemporaneous hematopoietic progenitors and HSCs during zebrafish development. (**A**) UMAP showing expression of the gene *myb* across all cells, with enrichment in HSPCs clusters (dotted line). The *myb* expressing population contains proliferating cells representing a mix of identities. (**B**) UMAP of the HSPC subset circled in (A). (**C**) Heatmap of differentially expressed genes of HSCs compared to EryPs (left), MyPs (middle), and LyPs (right). (**D**) UMAP showing the HSPC populations at 1 dpl, 6 dpf, and 10 dpf. (**E**) Gene enrichment analysis of HSCs, LyPs, and MyPs at the developmental timepoints indicated using EnrichGO for Biological Processes. Number in parentheses indicate the number of genes differentially expressed. Comparison was done between two timepoints, and top DEGs with greater than 1.5-fold effect were used for the enrichment analysis. (**F**) Confocal imaging of mCherry signal in the CHT at one-day-post labeling for early-, mid-, and late-HSPC showing highest signal from the early labeling (2 dpf) compared to later. Quantification of the number of mCherry+ cells in the CHT shown on right. (**G**) UMAP showing HSPCs at one-day post labeling (1 dpl, left) and their relative percentages in the bar plot (right).

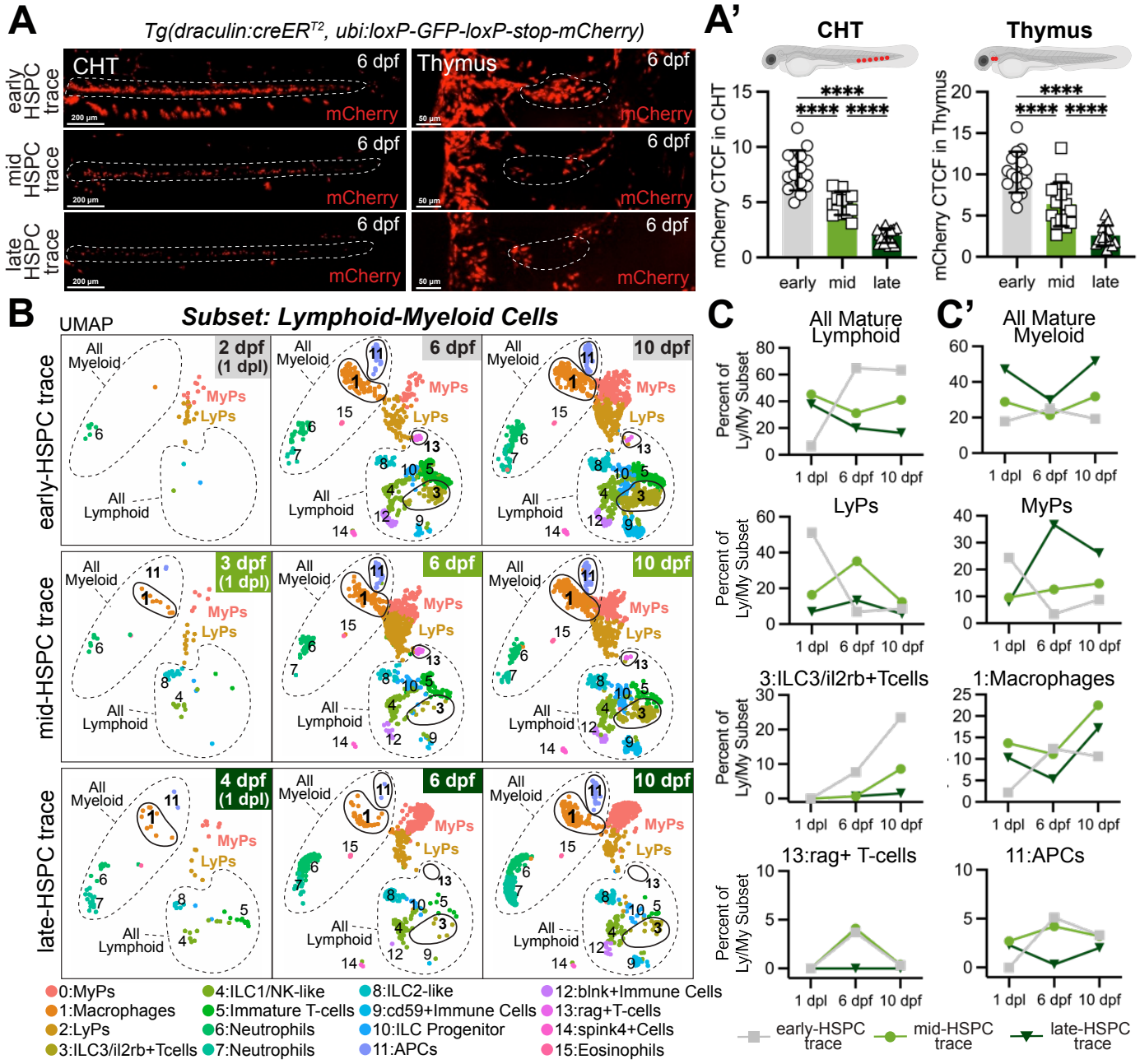
A
Tg(draculin:creER^{T2}, ubi:loxP-GFP-loxP-stop-mCherry)
early HSPC trace
mid HSPC trace
late HSPC trace
CHT
Thymus
6 dpf
mCherry
200 µm
50 µm
A'
CHT
Thymus
mCherry CTCF in CHT
mCherry CTCF in Thymus
****
early
mid
late
B
UMAP
Subset: Lymphoid-Myeloid Cells
early-HSPC trace
mid-HSPC trace
late-HSPC trace
2 dpf (1 dpl)
3 dpf (1 dpl)
4 dpf (1 dpl)
6 dpf
10 dpf
All Myeloid
All Lymphoid
MyPs
LyPs
0:MyPs
1:Macrophages
2:LyPs
3:ILC3/il2rb+Tcells
4:ILC1/NK-like
5:Immature T-cells
6:Neutrophils
7:Neutrophils
8:ILC2-like
9:cd59+Immune Cells
10:ILC Progenitor
11:APCs
12:blnk+Immune Cells
13:rag+T-cells
14:spink4+Cells
15:Eosinophils
C
All Mature Lymphoid
C'
All Mature Myeloid
LyPs
MyPs
3:ILC3/il2rb+Tcells
1:Macrophages
13:rag+ T-cells
11:APCs
Percent of Ly/My Subset
1 dpl
6 dpf
10 dpf
early-HSPC trace
mid-HSPC trace
late-HSPC trace
D
Differentially Expressed Gene Analysis at 10 dpf
Early HSPC trace
Mid HSPC trace
Late HSPC trace
Analysis #1
Analysis #2
Analysis #3
enrichGO analysis for Biological Processes
D'
1:Macrophages at 10 dpf
6:Neutrophils at 10 dpf
hydrogen peroxide catabolic process
hydrogen peroxide metabolic process
reactive oxygen species metabolic process
canonical NF–kappaB signal transduction
macrophage differentiation
myeloid leukocyte differentiation
response to xenobiotic stimulus
cell chemotaxis
positive regulation of cytosolic calcium ion concentration
non–canonical NF–kappaB signal transduction
tumor necrosis factor–mediated signaling pathway
response to cytokine
actin filament organization
neutrophil chemotaxis
regulation of cytoskeleton organization
Up in Early (#3)
Up in Mid (#2)
Up in Late (#2)
p.adjust
GeneRatio

Figure 3. Lympho-myelo lineage differentiation kinetics vary across HSPC development. (**A**) Confocal imaging of mCherry signal in the CHT (left) and Thymus (right) derived from early, mid, and late HSPCs at 6 dpf and are circled with dotted white lines. (A') Quantification shows highest signal in thymus and CHT derived from early-HSPCs. (**B-B''**) UMAP showing the lymphoid-myeloid subset at 1 dpl, 6 dpf, and 10 dpf from the early (top), mid (middle), or late (bottom) HSPC trace. Dotted lines circle the myeloid lineage cells or lymphoid lineage cells. Solid lines circle the clusters of interest analyzed in B'-B'. In B' (lymphoid) and B'' (myeloid), plots show changes in percentages of cells per cluster in early- (gray), mid- (light green), and late-HSPC (dark green) traces. (**C**) To determine the differences between myeloid progeny derived from early, mid, and late HSPCs, we did differential gene expression followed by GO analyses of cells from 10 dpf larvae. (C') EnrichGO for Biological Processes enrichment analysis of upregulated genes in macrophages and neutrophils from the comparisons shown in C.

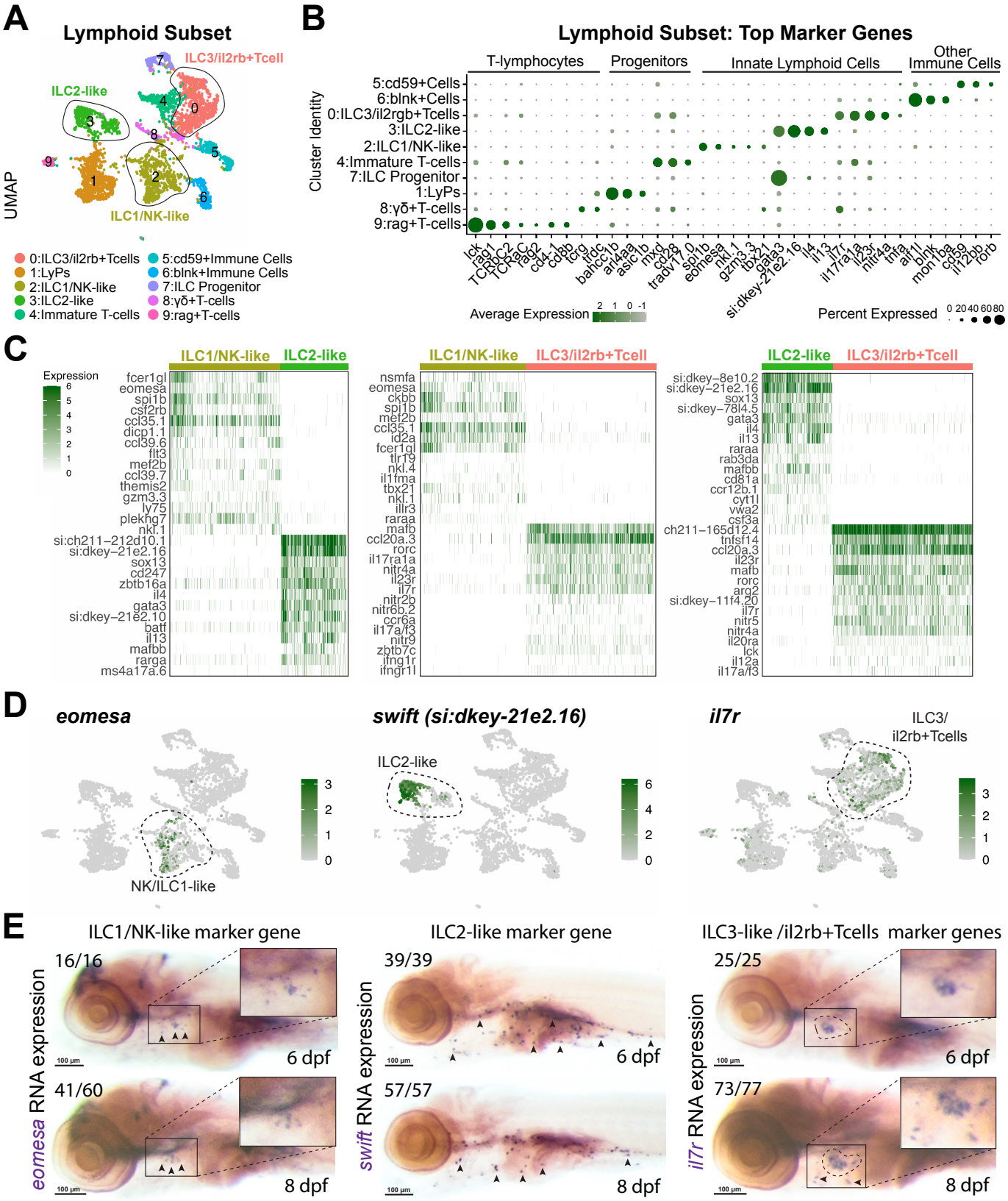

Figure 4. HSPCs generate a variety of lymphoid lineage cells during development. (**A**) UMAP showing lymphoid subset of data from Figure 1B. Circled populations highlight clusters containing the three types of ILC-like cells. (**B**) Dot plot shows selected top marker genes of each cluster generated

using the FindAllMarkers function in Seurat with Wilcoxon Rank Sum testing. (**C**) Heatmap of genes differentially expressed comparing the three ILC clusters to each other. (**D**) UMAP showing expression of *eomesa, si:dkey21e2.16, il7r*, that were selected for *in situ* hybridization testing for the three ILC-like populations. (**E**) Images of *in situ* RNA hybridization for selected marker genes of ILC-like cells at 6 and 8 dpf. Triangles point to puncta and dotted line circles the thymus. Inset shows enlarged image around the thymus.

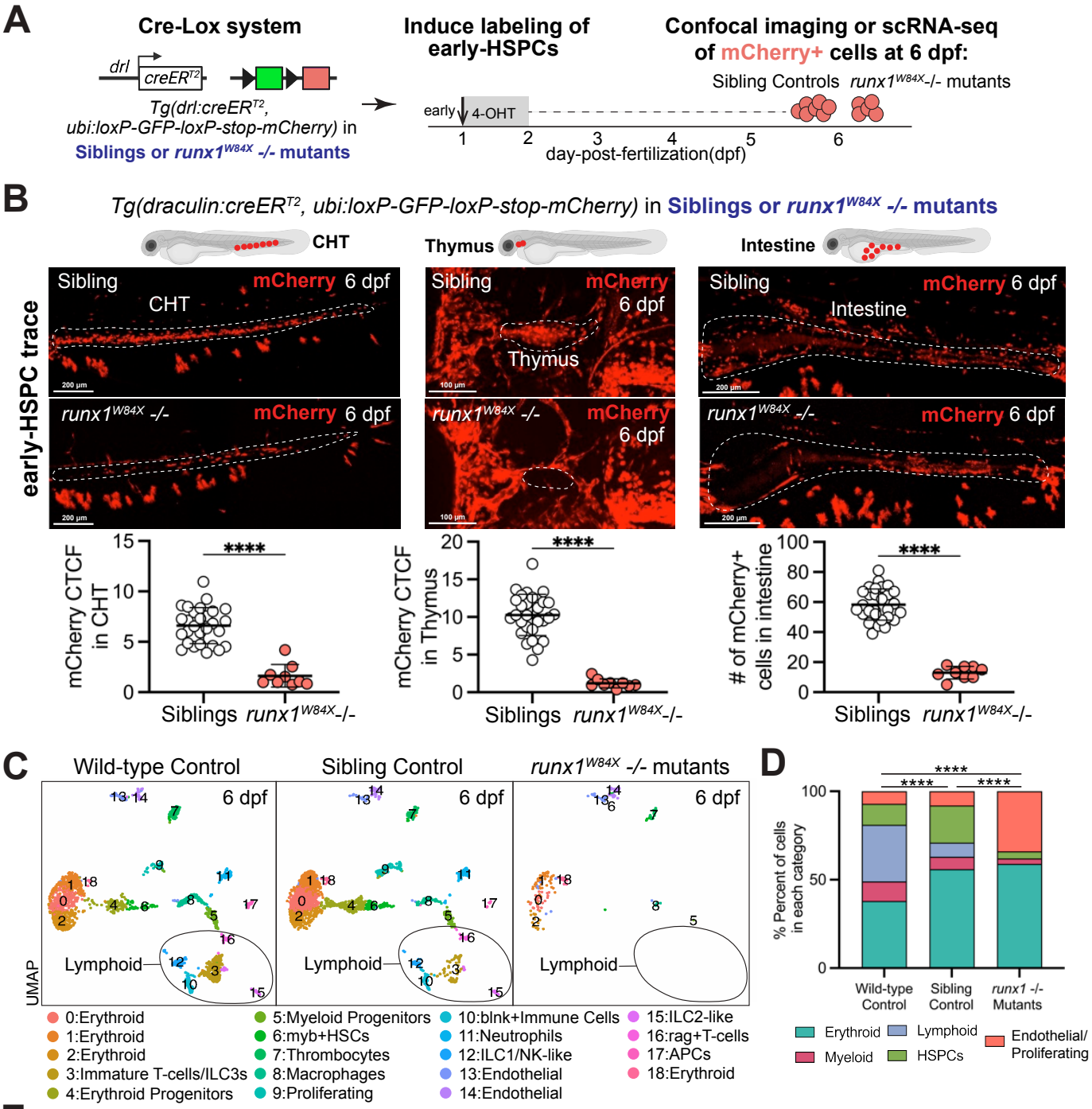
A
Cre-Lox system
drl
creER^{T2}
Tg(drl:creER^{T2}, ubi:loxP-GFP-loxP-stop-mCherry) in
Siblings or runx1^{W84X} -/- mutants
Induce labeling of early-HSPCs
Confocal imaging or scRNA-seq of mCherry+ cells at 6 dpf:
Sibling Controls
runx1^{W84X}-/- mutants
early
4-OHT
1 2 3 4 5 6
day-post-fertilization(dpf)
B
Tg(draculin:creER^{T2}, ubi:loxP-GFP-loxP-stop-mCherry) in Siblings or runx1^{W84X} -/- mutants
CHT
Thymus
Intestine
early-HSPC trace
Sibling
mCherry 6 dpf
runx1^{W84X} -/-
mCherry CTCF in CHT
mCherry CTCF in Thymus
# of mCherry+ cells in intestine
****
Siblings
runx1^{W84X}-/-
C
Wild-type Control
Sibling Control
runx1^{W84X} -/- mutants
6 dpf
UMAP
Lymphoid
0:Erythroid
1:Erythroid
2:Erythroid
3:Immature T-cells/ILC3s
4:Erythroid Progenitors
5:Myeloid Progenitors
6:myb+HSCs
7:Thrombocytes
8:Macrophages
9:Proliferating
10:blnk+Immune Cells
11:Neutrophils
12:ILC1/NK-like
13:Endothelial
14:Endothelial
15:ILC2-like
16:rag+T-cells
17:APCs
18:Erythroid
D
% Percent of cells in each category
Wild-type Control
Sibling Control
runx1 -/- Mutants
Erythroid
Lymphoid
Endothelial/ Proliferating
Myeloid
HSPCs
E
eomesa RNA at 6 dpf
swift RNA at 6 dpf
il7r RNA at 6 dpf
+/+
+/-
-/-
6 dpf
n=9
n=27
n=13
n=23
n=7
n=5
n=8
# of eomesa+ puncta
# of swift+ puncta
Thymus Signal (pixel intensity)
ns
runx1^{W84X}

Figure 5. Zebrafish ILCs depend on the function of Runx1. (**A**) Outline of experiment, where early-HSPC lineage tracing was done in *runx1*^{W84X} homozygous mutants and in sibling controls. Early-HSPCs were labeled at 1 dpf by addition of tamoxifen. At 6 dpf, larvae were either imaged or processed for scRNA-seq. (**B**) Confocal images showing mCherry signal derived from early-HSPCs in CHT (left), thymus (middle), and the intestines (right). Signal from early HSPC progeny is reduced in *runx1*^{W84X} homozygous mutants in all three locations. Quantification displayed below, where each dot represents the signal for an individual larva. (**C**) UMAP showing hematopoietic and endothelial cells from 6 dpf wild-type controls (early HSPC data from Figure 1), *runx1*^{W84X} siblings and homozygous mutants. Lymphoid lineage cells including ILCs are circled. (**D**) Bar plot shows percentage of cells when grouped by major hematopoietic categories. Erythroid includes clusters (7)Thrombocytes and (0,1,2,18)Erythroid. Myeloid category includes (8)Macrophages, (17)APCs, and (11)Neutrophils. Lymphoid category includes all the circled cells on the UMAP, clusters 3,10,12,15,16. HSPCs category includes clusters 4, 5, and 6. The “Other” category includes (13,14)Endothelial and (9)Proliferating cells. (**E**) *In situ* RNA hybridization of *eomesa*, *swift*, and *il7r* in *runx1*^{W84X} homozygous mutants. Images (left) are representative of the mean signal. Triangles point to quantified puncta, while dotted line circles the thymus. Quantification (right) shows significant reduction of all three ILC genes. Statistics: in (B) average ± std and p-values are calculated with an unpaired t-test.

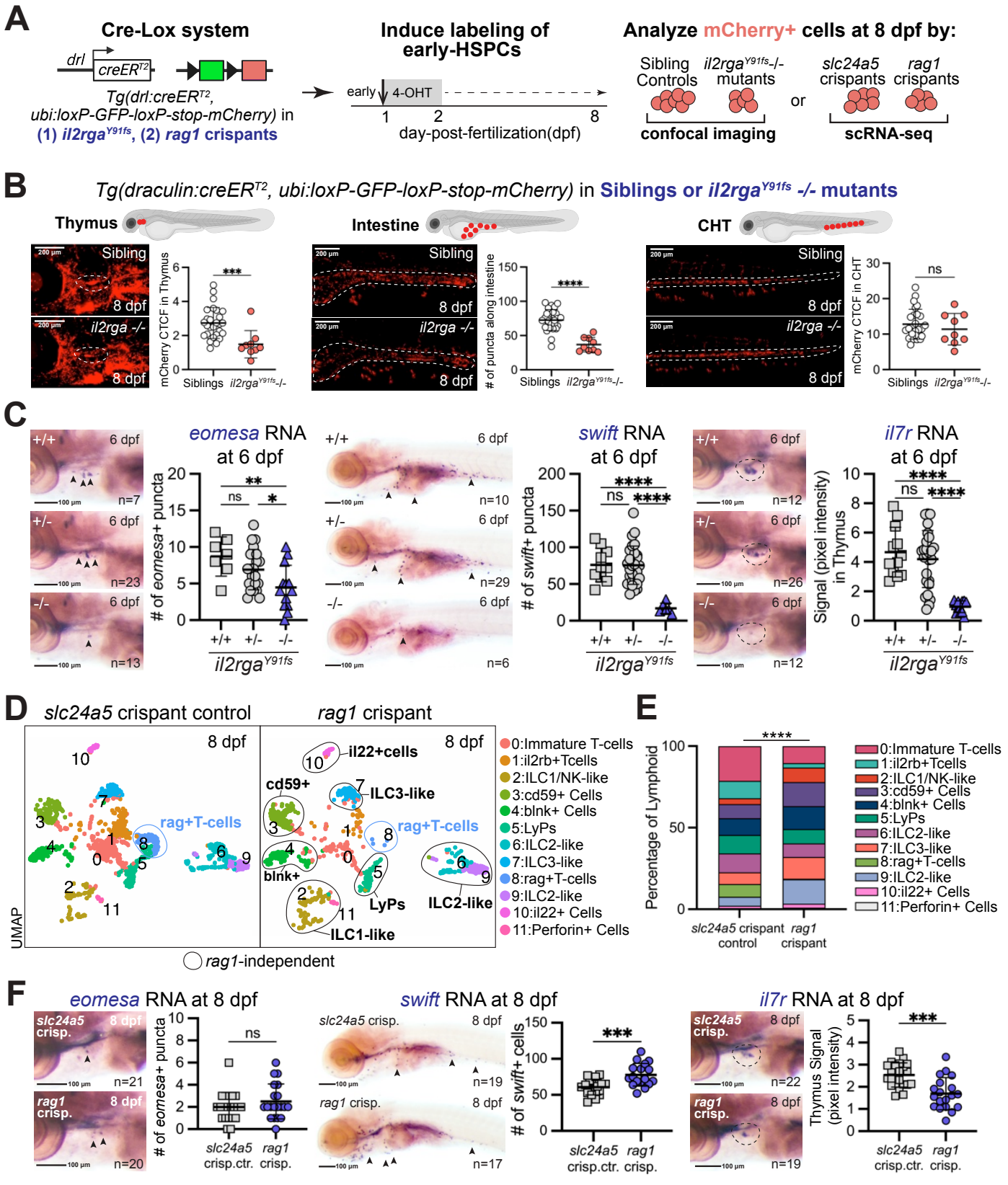

Figure 6. Zebrafish ILCs are Il2rga-dependent and Rag1-independent. (**A**) Outline of experiment of early-HSPC lineage tracing in *il2rga*^{Y91fs} mutants and in *rag1* crispants. The *il2rga*^{Y91fs} mutants were analyzed by confocal imaging and crispants were subject to scRNA-seq at 8 dpf. Both groups were

analyzed by *in situ* hybridization. As a control for CRISPR/Cas9 mutagenesis, we targeted the *slc24a5 golden* locus for the crispants experiment. (**B**) Confocal imaging of mCherry signal derived from early-HSPCs in siblings and *il2rga*^{Y91fs} homozygous mutants at 8 dpf in the thymus (left), intestine (middle), and CHT (right). Quantification shows significant decreases in all three locations in the *il2rga* mutants. (**C**) *In situ* RNA hybridization for ILC marker genes in 8 dpf larvae of all three *il2rga*^{Y91fs} genotypes. Triangles point to quantified puncta, while dotted line circles the thymus. Images (left) are representative of the mean signal. Quantification (right) shows all three ILC genes were decreased. (**D,D'**) UMAP showing the lymphoid subset of clusters detected in controls and *rag1* crispants in D. (D') The *rag1*-independent clusters are circled. Quantification of the percentage of cells in each cluster within the lymphoid subset shown in (D). See supplemental for absolute numbers. (**E**) *In situ* RNA hybridization for ILC marker genes in 8 dpf in controls and *rag1* crispants. Images (left) are representative of the mean signal. Triangles point to quantified puncta, while dotted line circles the thymus. Quantification (right) shows *eomesa* was unchanged, while *swift* was increased and *il7r* was decreased in the *rag1* crispants. Statistics: in (B,E) average ± std and p-values are calculated with an unpaired t-test.

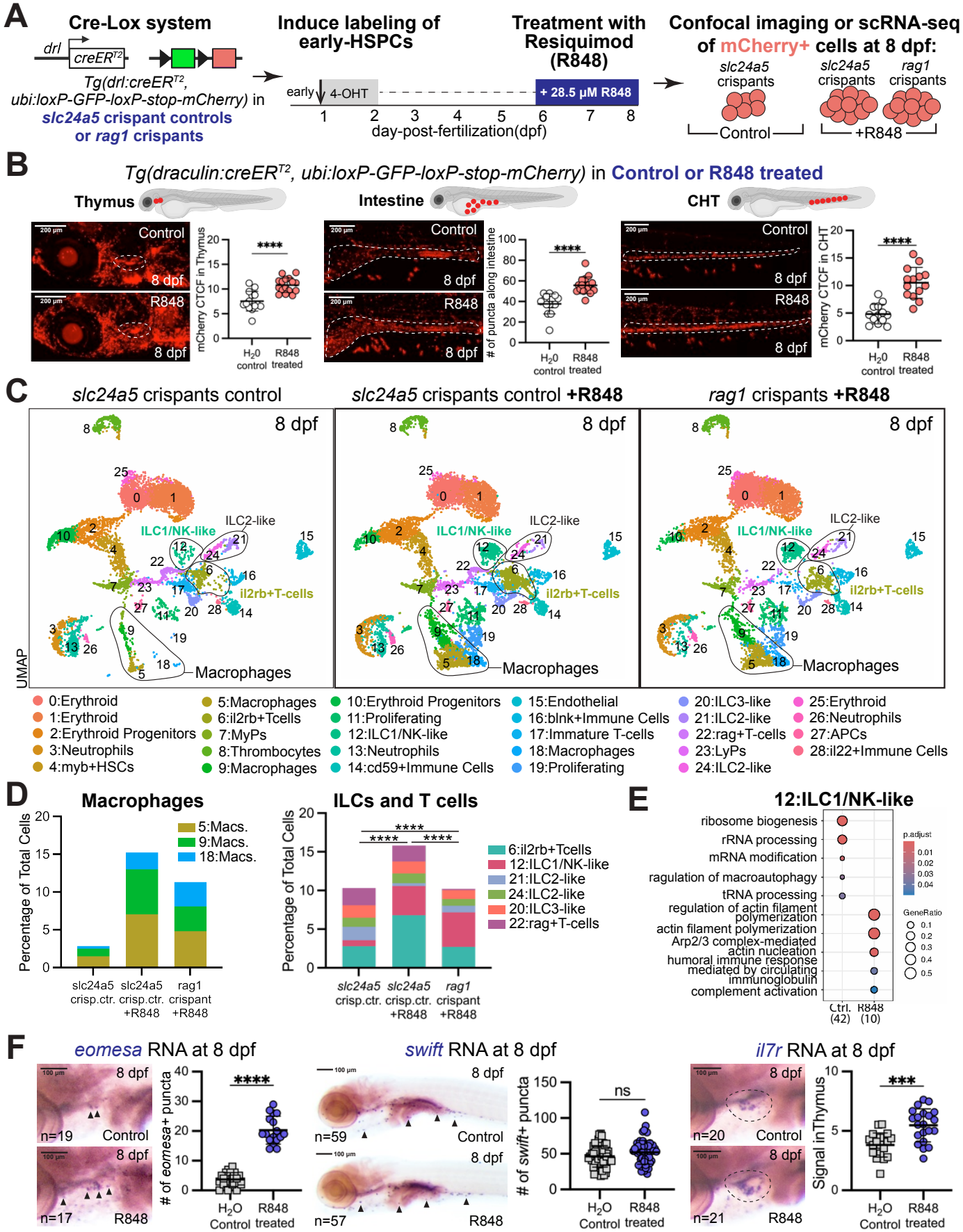
A
Cre-Lox system
drl
creER^{T2}
Tg(drl:creER^{T2}, ubi:loxP-GFP-loxP-stop-mCherry) in slc24a5 crispant controls or rag1 crispants
Induce labeling of early-HSPCs
early
4-OHT
+ 28.5 µM R848
1 2 3 4 5 6 7 8
day-post-fertilization(dpf)
Treatment with Resiquimod (R848)
Confocal imaging or scRNA-seq of mCherry+ cells at 8 dpf:
slc24a5 crispants
slc24a5 crispants
rag1 crispants
Control
+R848
B
Tg(draculin:creER^{T2}, ubi:loxP-GFP-loxP-stop-mCherry) in Control or R848 treated
Thymus
Intestine
CHT
Control
R848
8 dpf
mCherry CTCF in Thymus
# of puncta along intestine
mCherry CTCF in CHT
****
H$_2$0 control
R848 treated
C
slc24a5 crispants control
slc24a5 crispants control +R848
rag1 crispants +R848
8 dpf
UMAP
ILC1/NK-like
ILC2-like
il2rb+T-cells
Macrophages
0:Erythroid
1:Erythroid
2:Erythroid Progenitors
3:Neutrophils
4:myb+HSCs
5:Macrophages
6:il2rb+Tcells
7:MyPs
8:Thrombocytes
9:Macrophages
10:Erythroid Progenitors
11:Proliferating
12:ILC1/NK-like
13:Neutrophils
14:cd59+Immune Cells
15:Endothelial
16:blnk+Immune Cells
17:Immature T-cells
18:Macrophages
19:Proliferating
20:ILC3-like
21:ILC2-like
22:rag+T-cells
23:LyPs
24:ILC2-like
25:Erythroid
26:Neutrophils
27:APCs
28:il22+Immune Cells
D
Macrophages
Percentage of Total Cells
5:Macs.
9:Macs.
18:Macs.
slc24a5 crisp.ctr.
slc24a5 crisp.ctr. +R848
rag1 crispant +R848
ILCs and T cells
6:il2rb+Tcells
12:ILC1/NK-like
21:ILC2-like
24:ILC2-like
20:ILC3-like
22:rag+T-cells
E
12:ILC1/NK-like
ribosome biogenesis
rRNA processing
mRNA modification
ragulation of macroautophagy
tRNA processing
regulation of actin filament polymerization
actin filament polymerization
Arp2/3 complex-mediated actin nucleation
humoral immune response mediated by circulating immunoglobulin
complement activation
p.adjust
GeneRatio
Ctrl. (42)
R848 (10)
F
eomesa RNA at 8 dpf
swift RNA at 8 dpf
il7r RNA at 8 dpf
n=19
n=17
n=59
n=57
n=20
n=21
# of eomesa+ puncta
# of swift+ puncta
Signal inThymus
ns
***

Figure 7. Viral mimicry stimulates ILC-like cell expansion in zebrafish larvae. (A) Outline of experiment exploring the impact of viral mimicry on the larval immune cell landscape. Crispants for *slc24a5* (control) and *rag1* were treated with either vehicle control or 28.5μM R848 from 6-8 dpf and mCherry+ cells from each condition were sequenced at 8 dpf. (**B**) Confocal imaging of early-HSPCs derived mCherry+ cells in the thymus (left), intestine (middle), and CHT (right) at 8 dpf in controls and R848-treated larvae. Images (left) are representative of the mean signal. Quantification (right) shows increased mCherry+ signal in all three locations. (**C**) UMAP showing all hematopoietic clusters detected at 8 dpf per condition. Clusters showing substantial expansion upon R848 treatment are circled. Clusters 11 and 19 are not circled as they contains proliferating cells representing a mix of identities. (**D**) Bar plots show the percentages of cells in macrophage or the ILC/T-cell clusters. Percentages are relative to all the cells shown in UMAP in (C), see supplemental for absolute numbers. (**E**) Gene enrichment analysis using EnrichGO for Biological Processes on genes upregulated in ILC1/NK-like cluster in response to R848 treatment showing enrichment in cytokine and chemokine activity. (**F**) *In situ* RNA hybridization for ILC genes in control and R848 treated 8 dpf larvae. Triangles point to quantified puncta, while dotted line circles the thymus. Images (left) are representative of the mean signal. Quantification (right) shows no change in *swift* levels and significant increases in *eomesa* and *il7r*. Statistics: in (B,F) average ± std and p-values calculated with an unpaired t-test.